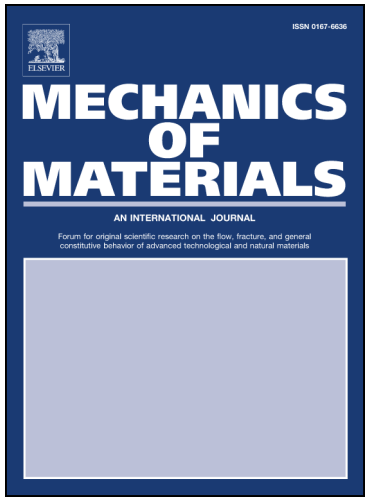

Large Strain Compressive Response of 2-D Periodic Representative Volume Element for Random Foam Microstructures

J. Alsayednoor, P. Harrison, Z. Guo

PII: S0167-6636(13)00118-X
DOI: http://dx.doi.org/10.1016/j.mechmat.2013.06.006
Reference: MECMAT 2140

To appear in: *Mechanics of Materials*

Received Date: 27 August 2012
Revised Date: 21 April 2013

Please cite this article as: Alsayednoor, J., Harrison, P., Guo, Z., Large Strain Compressive Response of 2-D Periodic Representative Volume Element for Random Foam Microstructures, *Mechanics of Materials* (2013), doi: http://dx.doi.org/10.1016/j.mechmat.2013.06.006

Large Strain Compressive Response of 2-D Periodic Representative Volume Element for Random Foam Microstructures

Alsayednoor, J.[1], Harrison, P.[1*] and Guo, Z.[2]

[1] School of Engineering, University of Glasgow, University Avenue, G12 8QQ Glasgow, UK

[2] Department of Engineering Mechanics, Chongqing University, Chongqing 400044, China

corresponding author, fax: 0141 3304343, telephone: 0141 3304318,

Email: Philip.harrison@glasgow.ac.uk

ABSTRACT

A numerical investigation has been conducted to determine the influence of Representative Volume Element (RVE) size and degree of irregularity of polymer foam microstructure on its compressive mechanical properties, including stiffness, plateau stress and onset strain of densification. Periodic two-dimensional RVEs have been generated using a Voronoi-based numerical algorithm and compressed. Importantly, self-contact of the foam's internal microstructure has been incorporated through the use of shell elements, allowing simulation of the foam well into the densification stage of compression; strains of up to 80 percent are applied. Results suggest that the stiffness of the foam RVE is relatively insensitive to RVE size but tends to soften as the degree of irregularity increases. Both the shape of the plateau stress and the onset strain of densification are sensitive to both the RVE size and degree of irregularity. Increasing the RVE size and decreasing the degree of irregularity both tend to result in a decrease of the gradient of the plateau

region, while increasing the RVE size and degree of irregularity both tend to decrease the onset strain of densification. Finally, a method of predicting the onset strain of densification to an accuracy of about 10 per cent, while reducing the computational cost by two orders of magnitude is suggested.

Keywords: foam, micro-macro, RVE, PBC, contact

1 INTRODUCTION

Foams are an important class of engineering material used in a wide range of mechanical applications including lightweight sandwich structures where high specific stiffness and strength are important in the sandwich core, as flexible cushions to distribute pressure loads **(Miltz and Ramon, 1990)**, and as impact energy absorbers where they are often used to limit the transmission of inertial forces **(Mills et al. 2003)**. The microstructure of foam is fundamental in determining its bulk mechanical response. Consequently, a large body of work has been dedicated to understanding the relationship between microstructure and macro-scale properties of these materials. Computational homogenisation provides a powerful tool to investigate this relationship. Importantly, since the technique can include significant geometric changes of the material structure across the length scales, it is applicable to the study of materials undergoing large deformations **(Hardenacke and Hohe, 2009)**. Cellular materials, such as polymer and metal foams, are obvious candidates for analysis using this technique, due to their common use in impact and cushioning applications where large deformations are anticipated and are typically included at the product design stage.

Ideally, micro to macro **(Laroussi et al. 2002; Zhou and Soboyejo, 2004; Dillard et al. 2006)**, or meso to macro **(Boubakar et al. 2002)** simulation strategies can lead to significant time and cost savings typically incurred during experimental characterisation, where virtual testing is intended to replace the majority of the experimental test matrix. The technique can also be applied in material optimisation by informing manufacture processes in order to induce beneficial changes in a material's micro **(Duarte and Banhart, 2000; Blazy et al. 2004; Wouterson et al. 2005)** or meso-structure **(Boisse et al. 2011)**.

The concept of a Representative Volume Element (RVE) **(Hill, 1963)** employed in combination with a Periodic Boundary Condition applied along its edges **(Guedes and Kikuchi, 1990; Anthoine, 1995)** is often used to obtain a homogenised macro-response for a material's bulk behaviour. Here, the volume averaged deformation gradient across the RVE is determined from the displacement of its surface, likewise the volume averaged nominal stress is computed in terms of the nominal stress on its surface. Once these volume averaged behaviours are determined they can be used either in parameter fitting for continuum-based constitutive models **(Guo et al. 2012)**, or more directly, using a micro-to-macro simulation strategy **(Miehe and Koch, 2002; Hohe and Becker, 2003)**.

The accuracy and practicality of computational homogenisation depends on the use of RVEs that are both realistic and computationally efficient, two criteria that are often at odds with one another **(Kouznotsova et al. 2001;**

Smit et al. 1998; Swan, 1994). The size of the RVE and its level of detail are two important considerations. For materials based on a regularly repeating micro or mesoscale structure, such as a honeycomb core or a woven textile, the choice of RVE size is usually trivial, and can be taken as the repeat unit cell within the material **(Smit, 1998)** (though this choice precludes the prediction of deformations with wavelengths longer than the size of the repeat unit cell). When it comes to materials possessing random micro-structures, in general, the larger the RVE the more microscopic structural information it will contain. Ideally, an RVE model should be sufficiently large to be statistically representative of the composite **(Drugan and Willis, 1996)** while small in comparison to the larger structure. However, restrictions on computational resources impose practical limitations on the size of the RVE and so the model should instead be chosen such that it can predict the overall response within a desired accuracy. To the best of the authors' knowledge, there is no analytical method of predicting the minimum RVE size for cellular structures undergoing large deformations. An important aim of this work is therefore to investigate the effects of changing the RVE size, as a function of the property under investigation (and consequently the level of compression) and the degree of irregularity within the RVE model.

When it comes to the level of detail within the RVE model, one extreme strategy is to employ RVEs based on, for example, actual 3-D topologies, measured using techniques such as micro-CT imaging **(Shan and Gokhale, 2001; Maire et al. 2003; Michailidis et al. 2011).** In this case, issues associated with strict application of the PBC have to be resolved **(Youssef et**

al. 2005) and long simulation times associated with the large number of continuum elements in the RVE currently restrict practical application for complex structures. The other extreme involves significant simplifications in the material's microstructure, involving various measures such as the use of numerical algorithms to generate analogous microstructures **(Zhu et al. 2000; Korner et al. 2002; Roberts and Garboczi, 2002; Kraynik et al. 2003)**, minimisation of the size of the RVE, reduction in the dimensionality of the problem and use of structural elements, such as beam or shell rather than continuum elements **(Chen et al. 1999; Fazekas et al. 2002; Schmidt, 2004)**. Most researchers strike a compromise between these extremes in order to produce predictions of acceptable accuracy and reasonable speed **(Jang et al. 2008; Jang et al. 2010)**.

A recognised method of generating representative microstructures is through Voronoi tessellation **(Voronoi, 1908)**. This numerical technique provides a fast and effective method to create beam-based finite element microstructures of geometry similar to those of several classes of polymeric and metallic open and closed cell foams **(Silva et al. 1995; Van Der Burg et al. 1997; Shulmeister et al. 1998; Zhu et al. 2000)**. The method has been used previously to generate RVE models with a PBC for parametric investigations into the effects of factors such as structural variability, relative density and beam cross-section, on the macro-scale response of the foam **(Zhu et al. 2000; Zhu and Windle, 2002; Kraynik et al. 2004; Gong et al. 2005; Kraynik, 2006).**

Typically, the mechanical behaviour of foams under compressive strain can be classified into three distinct regions: the linear, plateau and densification regimes **(Gibson and Ashby, 1997)**. All the aforementioned investigations incorporating a PBC have been limited to the linear and plateau regions due to the absence of self-contact within the structure. Others have included self-contact in order to simulate the impact response of foam while including the effect of densification **(Zheng et al. 2005; Li et al. 2007; Borovinsek and Ren, 2008; Song et al. 2010).** These simulations were conducted without application of a PBC, a necessary omission due to the inertial response induced during high rate impacts. Thus, the latter were effectively simulations of simple macro-scale structures incorporating detail at the micro-scale. To the best of the authors' knowledge, there have been no investigations reported in the literature that consider the large-strain compressive behaviour of either a two or three-dimensional beam-based RVE that incorporate both self-contact and a periodic boundary condition. Here, a method of simultaneously including both of these features in two-dimensional RVEs, using a commercial FE code is demonstrated.

While a two-dimensional representation is a major simplification compared to real foams, the work is nevertheless a first step towards the development of the same strategy in a full three-dimensional model. Further, by first considering the problem in two dimensions, and then later in three dimensions, an intention is to determine which information, if any, translates from the much less computationally intensive two dimensional case to the three dimensional case. For example, transferable conclusions regarding

trends in the optimum RVE size in 2-D could potentially lead to large savings in computation time when considering 3-D RVEs.

The structure of the rest of the paper is as follows: In Section 2, the finite element model is outlined and the method of generating RVEs with a quantified degree of irregularity, a periodic structure and a periodic boundary condition is described. The method of modelling contact, which involves the use of equivalent beam-like shell elements, is discussed. Section 3 describes the methods of analysis that are applied in interpreting results. The latter are presented in Section 4 and conclusions are given in Section 5.

2 FINITE ELEMENT MODEL

A common practice when constructing RVEs for foam materials is to use structural beam and shell elements to produce significant reductions in computational cost. Beam elements are particularly well-suited to modelling the cellular rib structures of open cell foams **(Laroussi et al. 2002, Li et al. 2006[a])** and simulations of non-periodic beam-based models involving self-contact, have been demonstrated previously using commercial finite element software, e.g. LSDYNA^{TM} **(Borovinsek and Ren, 2008).** In this investigation the commercial FE code, Abaqus (Standard^{TM} and Explicit^{TM}) has been chosen for several reasons though mainly due to familiarity and the future intention to incorporate a material model already defined in an Abaqus user-subroutine. Nevertheless, this poses a difficulty in that while beam elements can detect contact in Abaqus, preliminary simulations using the Explicit^{TM} code (v6.7) suggest mesh penetration is a significant problem and very high

mesh densities are required on order to attain reasonable results. However, without the inclusion of self-contact within the RVE, it is impossible to investigate important material properties such as the true form of the plateau stress at high strains, onset strain of densification **(Li et al. 2006b)** and foam stresses during densification. To overcome the restrictions of using beam elements, contact has been modelled using equivalent three-dimensional quadrilateral shell elements; an approach found to be much more accurate than the use of beam elements. This strategy has been employed previously, for example, in simulations of honeycomb structures **(Honig and Stronge, 2002; Ruan et al. 2003)** and also in modelling the impact behaviour of two-dimensional, non-periodic cellular structures where the effects of impact velocity, relative density and cell-wall thickness on the structure's mechanical response have been analysed **(Zheng et al. 2005; Li et al. 2007; Zhang et al. 2010).** To do this, parameters of the shell elements must be adjusted in order to make the shell respond in the same manner as an equivalent beam element. The equivalence of beam and shell-based RVEs is discussed and demonstrated in Appendix A.

2.1 Generating a 2-D beam-based RVE with a random periodic structure

Various methods have been reported for the generation of foam-like RVEs based on Voronoi tessellation. The methods tend to differ in how the position of seed-points, required by the Voronoi tessellation algorithm, are generated **(e.g**. **Van der Burg et al. 1997; Grenestedt and Tanaka 1998; Silva and Gibson, 1997; Zhu et al. 2001[b])**. Here, a combination of methods proposed

by **Zhu et al. 2001[b]** and **Grenestedt and Tanaka 1998** is utilized. The method involves first generating a uniform distribution of seed positions, which correspond to the seeding of a perfectly regular honeycomb pattern. Next, a set of normally-distributed pseudo-random values are generated within a range with limits $\pm\Delta$. Here Δ is calculated by

$$\Delta = \frac{\alpha \times \delta_0}{100}, \quad \alpha \in (0,50) \tag{1}$$

where

$$\delta_0 = \sqrt{\frac{2A}{N\sqrt{3}}} \tag{2}$$

is the minimum distance between neighbouring seeds of a regular honeycomb cellular pattern in a closed area, *A* and *N* is the number of cells **(Zhu et al 2001[a])**. The parameter, α, controls the degree of irregularity within the RVE. These random values are added to the initial regular honeycomb seed positions (see Figure 1). This new technique has been found to be computationally faster than the method proposed by **Zhu et al. 2001[b]**, upon which it is based.

In order to generate a periodic two-dimensional RVE using this method, first a unit square is populated with regular seed positions (the precursor seeding for a honeycomb pattern). Equation (1) is then used to perturb these initial seed

positions to produce a unit square containing an irregular distribution of seeds. This 'perturbed' unit square seeding is copied nine times to create a larger square containing 3 x 3 identical perturbed unit square seedings. Applying a Voronoi tessellation algorithm to the resulting 3 x 3 structure produces a fully periodic cellular pattern within the central square, with pairs of counterpart nodes on opposing boundaries (see Figure 2). It is noted that for random materials, the RVE response should be isotropic **(Hill, 1963; Guedes and Kikuchi, 1990; Kruyt and Rothenburg, 2004)**. However, a honeycomb structure is slightly anisotropic, for example, simulations show the compressive stiffness along the 0^o orientation (and in each direction when the structure is rotated repeatedly by 60^o) is around 14% higher than that when the structure is compressed at 30^o (see Figure 5a). Consequently the honeycomb structure has a regular six-fold polar variation in stiffness. It follows that methods of generating Voronoi-based cellular structures by simply using a randomly perturbed honeycomb structure, result in RVE behaviour that begins with this six-fold symmetry in stiffness and gradually becomes more isotropic as the variability factor increases from zero, i.e. memory of the initial anisotropy is gradually erased as the value of the variability factor is increased. Methods of correcting this anomaly are possible and will be the subject of future work.

2.2 Boundary Condition on RVE

According to **Chen et al. 1999** a PBC produces an intermediate stiffness response, lower than a Prescribed Displacement Condition but higher than a Mixed Boundary Condition when applied to two-dimensional cellular

structured RVEs, consequently the PBC is considered the best compromise and has been adopted in this investigation. The concepts of a Representative Volume Element (RVE) and a Periodic Boundary Condition (PBC) are intrinsically linked. To apply a PBC on any two or three dimensional RVE, the structure must be fully periodic, meaning that a node on one boundary must have a counterpart at the same horizontal (on sides) or vertical (on top/bottom) position along the opposite boundary, see Figure 3, where the superscripts *L*, *R* , *T* and *B* indicate the left, right, top and bottom boundaries, respectively. A two dimensional PBC requires that: *(1) The motion of counterpart nodes on each pair of RVE boundaries are constrained to each other* and *(2) Stress continuity across boundaries is preserved.* For example, considering the first condition and referring to nodes along the side boundaries of the RVE shown in Figure 3b,

$$U_i^R = U_i^L + U_i^{d_i} \qquad i = 1 \ to \ 2 \tag{3}$$

$$U_i^R = U_i^L \ , \ U_i^T = U_i^B \qquad i = 3 \tag{4}$$

where *U* is the nodal displacement in the *i*th direction, the subscript, *i*, represents the degree of freedom with *i=1,2* indicating displacements in the *X* and *Y* directions and *i=3* indicating rotation perpendicular to the *X*-*Y* plane. In order to implement the PBC, the 'EQUATION' keyword option available in Abaqus™ has been employed. Two dummy nodes are generated, indicated in Equation (3) by the superscript d_i. The second condition implies the traction

vector acting on opposing boundaries of the RVE is equal and opposite at all counterpart points. Using two side nodes as an example,

$$\sigma^R.\mathrm{n}^R\left(\Gamma^R\right)=-\sigma^L.\mathrm{n}^L\left(\Gamma^L\right) \quad (5)$$

where the unit vectors $\mathrm{n}^R\left(\Gamma^R\right)$ and $\mathrm{n}^L\left(\Gamma^L\right)$ are normal to the right and left boundaries at the location of the nodes. The motion of the dummy node controlling the relative displacement of the horizontal edges of the RVE is prescribed according to the imposed compression strain (and the size of the RVE) while the motion of the dummy node controlling the displacement of the vertical edges of the RVE is determined by the FE code in order to maintain stress equilibrium across the vertical boundaries. No loads are imposed on the RVE by the user. Stress continuity at the boundaries when imposing a PBC is discussed in detail by **Smit et al., 1998**.

2.3 Beam-based RVEs

When modelling aluminium open cell foam using a small 3-D RVE and solid elements, the effect of variations of rib cross-sectional shape and area, as a function of length along the rib, have been found previously to be of diminishing importance with decreasing foam relative density **(Gong et al. 2005; Jang et al. 2008)**. Since only low-density open cell foams are considered in the current investigation (ρ_R =0.05), use of beam structures of constant cross-section is a reasonable approximation. For small strain simulations with no self-contact within the structure each rib of each cell has been modelled using five equal length 2-D Timoshenko quadratic beam

elements (B21 type element in Abaqus^{TM}) with a constant square cross-section of side-length, t. The latter is calculated using Equation (6) which relates *t*, to the relative density, ρ_R, and total length of the elements within the RVE **(Zhu et al. 2001[a])**:

$$t = \frac{\rho_R a}{\sum_{k=1}^{n} l_k} \tag{6}$$

where *n* is the number of elements, *a* is the area of RVE and *l* is the length of each individual element. For all cases, the material model is linear elastic with a Young's modulus, E_S of 1GPa, material density, ρ_m of 2000 kgm^{-3} and Poisson's ratio = 0.33 consequently it should be noted that all conclusions from this work are restricted to linear elastic behaviour of the constituent material. More realistic material behaviour will be included in future work in order to determine if behaviours such as plastic yielding or strain hardening significantly affect the generic findings of this work. The Timoshenko beam element formulation is capable of including the effects of transverse shear stiffness for thick section beams (recommended for cross section diameters up to 1/8th of the structures axial length) and converges on the slender element result (zero-transverse shear stiffness) for elements where the cross-section diameter is less than about 1/15th of the beam's axial length **(Abaqus User Manual v6.9)**. The error in the structural element approximation progressively increases at a faster rate as the thickness/length ratio increases and inevitably leads to some error. The foam density in this investigation is

close to the upper limit of what can be feasibly considered using structural elements for 2-D RVEs without causing excessively large errors due to high rib thickness/length ratios. For the perfectly regular honeycomb structure, a relative density of 0.05 in Equation (6) leads to ratios of about 1/7. For random RVEs this ratio varies from rib to rib due to changing rib lengths and use of a constant rib thickness throughout the RVE. The average value of the ratio falls to about 1/25 for the most irregular case, though here a small proportion of the ribs have ratios significantly higher than 1/8. Future work will focus on either quantifying this error or implementing techniques to reduce possible error, such as imposing a maximum ratio when generating the RVE. All element cross-section properties are assigned prior to the analyses and remain constant during deformation. In the versions of Abaqus used in this investigation (up to and including version 6.12), contact detection between shell elements has been found to be significantly more reliable (less penetration) than contact detection between beam elements. Consequently, for larger strain simulations involving self-contact between the beam structures within the RVE, beam elements have been replaced by equivalent shell element-based beam structures. The technique behind this change is described in Appendix A.

In order to facilitate generic comparison of results with those produced elsewhere **(e.g. Zhu et al. 2002)** a dimensionless 'reduced stress' is used throughout this investigation, see Equation (7) **(Zhu et al. 2006)** which allows comparison of stress results between RVEs of differing relative density and with different element modulus.

$$\sigma_R = \frac{\sigma}{E_S \rho_R^3} \tag{7}$$

3 ANALYSIS

Depending on the application, various material properties can be of interest when designing products incorporating foams, including stiffness, yield stress, length and form of the plateau region and onset strain of densification **(Li et al 2006[b])**. In addition, during the course of this investigation an additional material parameter has been identified; the contact strain. The latter has been found to be a very useful parameter in enhancing computational efficiency through guiding simulation strategy and through predicting the onset strain of densification using relatively small RVEs (see Section 4.2). Due to the gradually changing form of a typical foam's stress - strain curve, exact determination of these parameters can be difficult and so, in Section 3.1, brief descriptions of these properties and the methods used to determine their values is presented. Properties are considered in the following order: (i) the foam stiffness at small strains (< 5%), (ii) the form of the plateau stress and (iii) the onset strain of densification and the contact strain. Prior to discussing these results, Section 3.2 addresses some of the computational issues that have to be addressed in conducting this investigation.

3.1 Property definitions

The behaviour of the cellular structures examined in this investigation is highly non-linear. The reduced stress – strain curves rarely show an initial small-

strain perfectly linear response due to the gradual yet early onset of bending and buckling of beams within the microstructure (see, for example, Video 1). Consequently, in order to determine the ***RVE stiffness***, the reduced secant modulus, a dimensionless quantity, is calculated at both 1% and 5% compressive strain. In contrast, defining equivalent representative quantities for the ***plateau region*** of the stress-strain curves is less straight forward and so only a qualitative comparison of the form of the reduced stress - strain curve is performed. The ***onset strain of densification*** is the point towards the end of the plateau region, at which the gradient of the stress – strain curve shows a sudden increase. It is a particularly important quantity when considering the behaviour of foams under large compressive strains such as in impact, packaging and cushioning applications. Following **Li et al 2006[b]**, the onset strain of densification can be identified consistently and objectively using the location of the maximum of the 'efficiency function', η, see Equation (8).

$$\eta(\varepsilon) = \frac{1}{\sigma(\varepsilon)} \int_{\varepsilon_y}^{\varepsilon} \sigma(\varepsilon) d\varepsilon \qquad (8)$$

where σ is stress, ε is strain and ε_y is the yield strain of the material (taken here at 10% strain). The ***contact strain*** introduced here, is very similar to the onset strain of densification though the use of computational modelling allows a more precise definition; i.e. the strain at which self-contact within the microstructure results in an increase of 5 per cent in the stress-strain response of the RVE, immediately prior to the permanent divergence of the

two curves as the strain increases, as compared to an identical RVE deforming without self-contact. It also differs to the onset strain of densification in the method by which it is determined. By conducting simulations both with and without contact, its location becomes apparent when directly comparing the subsequent reduced stress - strain curves; the two curves follow similar paths until a certain strain, after which the curves diverge (see Figure 4 and Video 1). Experience suggests that in most cases self-contact within the RVE microstructure usually starts after about 20% (minimum) compressive strain, though only begins to significantly affect the form of the reduced stress-strain curve at higher strains, i.e. at and after the contact strain.

3.2 Microstructural irregularity, RVE size and Computational Resource Considerations

To study the effect of the degree of irregularity four different values of α have been employed in generating RVEs (α = 0, 10, 20, 50). Examples are shown in Figure 5 where each image shows RVEs containing 150 cells; the smallest RVE size used in this investigation. The relative density of each RVE is kept constant however the total element length tends to increase with increasing degree of irregularity. Consequently, Equation (6) implies that the average thickness of the elements tends to decrease with increasing values of α.

Size effects have been explored using RVEs containing 150, 600, 1350 and 2400 cells which can be conveniently referred to as the sizes 1x150, 4x150, 9x150 and 16x150 (See Figure 6). Practical limitations on computational

resource mean that statistical investigations into the effect of RVE size on property predictions for all α values, and the effect of α value on property predictions for all RVE sizes would be prohibitively time consuming. To illustrate, Figure 7 shows the computation time versus RVE size for the explicit shell-based simulations (see Appendix A) including contact (simulations conducted using a 64 bit Windows with intel(R)Xeon(R) CPU @ 2.66GHz and 12GB RAM). A 16x150 cell simulation requires about 80 times longer than a 1x150 cell simulation and can take more than 35 hours to reach 80% compression – see Figure 7. To overcome this computational limitation it has been assumed that conclusions regarding the size effect on a given property produced using a degree of irregularity with α = 20, can be applied to RVEs with α = 0, 10 and 50, see Figure 5. Given that the degree of irregularity, α = 20, sits approximately midway between 0 and 50 this assumption is considered to be a reasonable compromise. This degree of irregularity is considered the most realistic representation of a two-dimensional slice of open-cellular polymer foam considered in this investigation (following preliminary visual comparison with actual micrographs of polymer foam cross sections). The strategy of extrapolating these conclusions on size effect to RVE behaviour generated using other α values means that simulations exploring the effect of changing α value can be performed with the smallest sized RVE (to reduce computational requirements) and the likely effect on predicted properties due to using this smallest RVE size can then be estimated.

4 RESULTS

This section investigates the influence of RVE size and degree of irregularity on material properties.

4.1 Small Strain Response of RVE

From experience, the contact strain always occurs at more than 30% compressive strain (sometimes not until about 60% depending primarily on the degree of irregularity – see Section 4.2). As such, property predictions such as stiffness, made at less than 30% compressive strains do not need to include contact. In these cases, as the implicit method is more accurate and potentially faster than the explicit method when self-contact within the RVE is neglected, stiffness predictions have been made with the implicit static general method using beam elements. In order to maintain a standard protocol throughout this investigation, the same number of simulations has been used to analyse the small strain stiffness of the RVE as with the large strain properties (see Section 4.2). As such, aside from the case of the perfectly regular RVE (α = 0) which is calculated from a single simulation, all other results presented in Figures 8 to 13 are an average of either 15 simulations (α = 10 & 20) or 10 simulations (α = 50) and the full length of the error bars indicates one standard deviation in these results. As might be expected, in all cases the amount of variability between repeat results decreases as the size of the RVE is increased and increases with increasing degree of variability.

Figure 8 shows that RVE size has almost no effect on the average secant modulus calculated at 1% compression and at 5 % compression the average modulus increases only slightly, by about 4% as the RVE size increases from 1x150 to 16x150 cells. Also, RVE size has little effect on the averaged form of the reduced stress – strain curve at small strains, as demonstrated by the almost constant difference between the secant modulus determined at 1% and 5% compressive strain. These conclusions on the effects of changing RVE size suggest that the small RVE should provide accurate estimates for the average modulus at 1% compression, while slightly under predicting the average modulus at 5% compression, when compared to the larger RVE response.

Considering the effect of the degree of irregularity, Figure 9 shows that the modulus at 1% strain is almost unchanged as α increases from 0 to 50. In contrast, when considering the modulus at 5% compressive strain there is significant softening, by about 25%, when the degree of irregularity increases from α = 0 to 50. Perhaps conversely, **Zhu et al. 2001[a]** found the secant modulus calculated at 0.1% compressive strain increased with increasing degree of irregularity, though the extremely small strain used to calculate the modulus could possibly account for this difference in behaviour.

4.2 Large strain response of RVE

The plateau region usually begins at around 10% compressive strain and continues until the onset strain of densification. The reason behind the

yielding of the foam and the form of the plateau region is generally attributed to bending, buckling or torsion (for 3-D deformation) within the foam microstructure **(Banhart and Baumeister, 1998; Elliott et al. 2002; Jang et al. 2010)** (or some combination of all three mechanisms). Video 1 tends to corroborate this view, showing bending and buckling of the beam elements tends to begin at relatively low strains (around 10%) and a strongly non-linear response is predicted despite the use of a simple linear elastic material behaviour in the beam elements.

As explained in Section 3, the onset strain of densification is determined here using Equation (8). By definition, both the onset strain of densification and contact strain can only be predicted if self-contact within the RVE is modelled. It will be shown that the onset strain of densification always occurs at higher strains than the contact strain. In order to predict the onset strain of densification and contact strain the dynamic explicit method using shell-based RVEs with contact detection enabled has been employed (see Appendix A).

Examining first the form of the plateau stress, Figure 10 shows how the shape of the reduced stress - strain curve changes with RVE size. The plateau becomes flatter for larger RVEs with a slightly negative gradient developing between 20 to 35% strain. This is due to an increase in stress at around 20% strain along with a small decrease in stress between 30 to 40% strain with increasing RVE size. These conclusions suggest a small RVE can be expected to provide only an approximate estimate for the magnitude of the plateau stress and the form of the plateau may be less flat and lack the

slightly negative gradient seen in larger RVEs. Examining the effect of changing the degree of irregularity, Figure 11 shows that the form of the plateau region of the reduced stress – strain curve becomes less horizontal and more inclined as α increases, i.e. the foam behaves gradually less like an ideal energy absorbing material as the degree of irregularity increases. The small RVE size probably serves to exaggerate the size of this positive gradient but the general trend in behaviour remains clear; an increase in the degree of irregularity increases the size of the positive slope in the plateau region. **Zhu et al. 2006** made a similar comparison of the reduced stress-strain curves of two-dimensional beam-based RVEs with four different degree of irregularity (including honeycomb and Poisson Voronoi). Their results suggested that as irregularity increases, the level of the whole of the plateau stress decreases. In their investigation the RVE was constructed from about 60 cells and self-contact within the microstructure was not considered.

Examining now the onset strain of densification and contact strain, these are marked on the reduced stress – strain curves as 'OSD' and 'CS' in both Figures 10 and 11 and are also plotted as a function of RVE size in Figure 12 and as a function of degree of irregularity in Figure 13. Figures 10 and 12 show that for a given degree of irregularity (α = 20) the onset strain of densification decreases with increasing RVE size and converges towards the contact strain which remains almost constant with RVE size. This suggests that the onset strain of densification is more sensitive to the RVE size than the contact strain, an observation that prompts two interesting possibilities (i) *the contact strain of a small RVE could be used to predict the onset strain of*

densification in larger RVEs (ii) *the difference between the contact strain and onset strain of densification could be used to quantify the influence of RVE size; a large difference would suggest the RVE is too small and can be improved by increasing its size*. If point (i) were to prove correct, this would allow dramatic savings in computational resource when aiming to correctly predict the foam's onset strain of densification. For example, referring to Section 3.2, the smallest RVE simulations (1X150 cells) require only about $1/80^{th}$ of the time of the largest RVE simulations (16x150 cells). In order to find the contact strain in the quickest time, simulations using small RVEs must be conducted, both with and without contact. Simulations without contact are relatively fast and increase the overall computation time by around only 20 per cent. In addition to requiring longer simulation time, around 50 per cent of the largest RVE simulations (this figure depends on the degree of irregularity of the RVE) produce errors before reaching large compressive strains (due to excessively distorted elements) and have to be discarded. This discard rate effectively increases the overall computational time for the large RVEs to about 130 times that of the small RVE simulations. Thus, the time saving involved in using the contact strain of small RVEs to estimate the onset strain of densification for the large RVEs is around two orders of magnitude.

Now considering the effects of the degree of irregularity, Figures 11 and 13 show how the onset strain of densification remains almost constant as α increases while the contact strain significantly decreases. Results of Figure 11 and the open points in Figure 13 are all conducted using the smallest RVE

size of 1x150 cells and are therefore likely to be adversely influenced by size effects that have been shown to strongly affect both the form of the plateau region and the onset strain of densification.

A final set of 10 simulations was conducted using RVEs with the maximum degree of irregularity (α = 50) and using the largest RVE size. The resulting average reduced stress – strain curve is shown in Figure 14 and the corresponding onset strain of densification and contact strain found using this curve are plotted as filled points in Figure 13. This final set of simulations (using α = 50) is designed to see if the same trends in terms of size effect that were found using α = 20, also occur when using α = 50. The results plotted in Figure 13 and 14 show once again that (a) the low strain zone of the plateau region is increased in value, creating a lower stress-strain gradient along the length of the plateau region (b) the contact strain remains stationary when the RVE size is increased from 1x150 to 16x150 cells and (c) the onset strain of densification decreases, effectively moving towards the contact strain. In this case using α = 50, the decrease is not sufficiently large for the two strain measures to closely coincide even when using the largest RVE, though the result does suggest that the contact strain, which is again almost RVE size independent, could once again serve as a good indicator of the onset strain of densification, as suggested in point (i) above. According to point (ii), the result suggests that the largest RVE (16x150 cells) should be increased further still if the adverse influence of size effects is to be fully eliminated. Attempts to run 25x150 cell simulations with α = 50 were conducted in order to explore this possibility. However, due to the exponentially increasing computational power

requirement (now more than 400,000 seconds for a 5% strain increment for 25x150 cell RVE, leading to simulation times of more than 8 weeks for a single simulation with strains of 60% compression) and also due the more frequent production of simulation errors when using α = 50 due to distorted elements, a rigorous stochastic investigation could not be performed without a significant increase in computational resource. This final investigation is therefore deferred to future work, when access to high performance super-computing facilities is anticipated.

5 CONCLUSIONS

Two-dimensional beam-based RVEs with different size and degree of irregularity have been generated using a Voronoi tessellation method. The inclusion of self-contact within the microstructure in the simulations has permitted the mechanical response of the RVEs to be investigated to very high compression strains, often greater than 80 per cent. To the best of the authors' knowledge, this is the first time that the analysis of important mechanical properties of structural foams, such as plateau shape and the onset strain of densification, have been investigated using a periodic RVE constructed using structural elements. Use of the latter means that simulation time is dramatically reduced compared to equivalent FE investigations using 3-D continuum elements to model the microstructure. Nevertheless, these large strain properties, which so far have been investigated using only linear elastic material behaviour, are shown to be sensitive to RVE size and ideally require large RVEs of at least 16x150 cells in order to eliminate size effects. This currently leads to long computation times (greater than 35 hours for 1

simulation using the current computer specification – see Section 3.2), which can be prohibitively costly when running multiple simulations in order to determine average stress-strain curves and stochastic variability between results. With this issue in mind, an important finding in this investigation is the discovery that the contact strain in a small RVE appears to be an excellent indicator of the onset strain of densification in a large RVE for degrees of irregularity of up to α = 20, and possibly for even higher values of microstructural irregularity. This finding can reduce computational requirements by a factor of around 100 times for these 2-D simulations. If this discovery holds true for 3-D simulations, then the savings in computation time are expected to be considerably greater still, a question that may form the subject of a future study.

ACKNOWLEDGEMENTS

The author's gratefully acknowledge funding from an EPSRC Doctoral Training Award to support this work.

Appendix A

A.1 Equivalent shell-based RVEs

Three dimensional general purpose linear shell elements with reduced integration (Type S4R element in Abaqus) have been used. As with the Timoshenko beam elements, (B21), transverse stiffness is considered and the behaviour of these elements converges to shear flexible theory for thick shells and to classical theory for thin shells (**Abaqus User Manual v6.9**). By appropriate adjustment of their structural and material parameters, the axial

and flexural mechanical response of beam and shell elements can be made equivalent. In this investigation, the thickness of beam and shell elements is equal while the width of the shell elements in the *Z* direction is 10 times the thickness, see Figure A1. Decreasing this factor results in faster simulation times but increases the risk of numerical convergence problems. Note that for reasons of computational efficiency this investigation aims to use structural elements throughout. Equivalent shell elements are therefore calibrated against beam elements rather than against a continuum element model of a beam in order to maintain the same underlying assumptions in the models and to therefore facilitate direct comparison of shell-element and beam-element based RVEs (see, for example, Section A.2).

Equations (A1) and (A2) are the main structural equations for the bending modulus of rectangular cross-section beam and shell elements for slender beams and thin shells.

$$q_{beam} = EI\frac{\partial^4 w}{\partial x^4}, \quad D_{beam} = EI \tag{A1}$$

$$q_{shell} = \frac{Eh^3}{12\left(1-\upsilon^2\right)}\nabla^4 w, \quad D_{shell} = \frac{Eh^3}{12\left(1-\upsilon^2\right)} \tag{A2}$$

where *q* is the applied load, *h* is the shell thickness, *w* is the deflection (of the beam/shell), υ is the Poisson's ration, *I* is the second moment of inertia of the beam, *E* is the Young's modulus and *D* represents the flexural rigidity of

beam/shell. The Poisson's ratio of the material, which is present in the shell formulation, see Equation (A2), is absent from the beam formulation **(Saada, 1974)** and so the shell's material Poisson's ratio must be set to 0 to produce an equivalent response as the beam elements. In addition, a structural element's 'effective section' Poisson's ratio controls the element's thickness behaviour as a result of axial or in-plane strains. As mentioned in Section 2.3, the beam's cross-sectional area is constant, implying a default effective section Poisson's ratio of *0*. In contrast, for shell elements, unless specified otherwise the element's effective section is predicted using Equation (A3) and can be chosen between *0* and *0.5*. **(Abaqus User Manual)**

$$\frac{t}{t_o} = \left(\frac{A}{A_o} \right)^{-\frac{\upsilon_s}{1-\upsilon_s}} \tag{A3}$$

where, υ_s, is the effective section Poisson's ratio, *t*, is the shell thickness and *A*, is the shell sectional area, the subscript *o* indicates the original value of *t* and *A*. In order to produce a constant cross-sectional area, as with the beam elements, υ_s is chosen as *0*. All nodal displacements are constrained to lie within the *X*-*Y* plane and nodal rotations are constrained about the *Z* axis only. By normalising the shell RVE force response by the shell width elongation factor (i.e. by dividing by 10), exactly the same mechanical response as an equivalent beam-based RVE (B21) is obtained. The following section of this appendix examines the correspondence between implicit and explicit simulations and issues related to computational resource before

A.2 Comparison between beam and equivalent shell-based RVEs

Preliminary simulations were conducted to assess the correspondence between implicit simulations employing beam elements and explicit simulations employing equivalent shell elements. An example result is shown in Figure A2, in this case applying 50% strain, using an RVE containing 150 cells with α = 0. Identical RVEs were used when drawing the comparison. Similar comparative tests on a range of RVEs (different sizes and irregularities) produced equally close results.

REFERENCES

ANTHOINE, A. 1995. Derivation of the Inplane Elastic Characteristics of Masonry through Homogenization Theory. International Journal of Solids and Structures, 32, 137-&.

AVALLE, M., BELINGARDI, G. & MONTANINI, R. 2001. Characterization of polymeric structural foams under compressive impact loading by means of energy-absorption diagram. International Journal of Impact Engineering, 25, 455-472.

BADCOCK, R. A., FERNANDO, G. F., HAYES, S. A., MARTIN, A. R. & NIGHTINGALE, C. 1995. Intensity based optical fibre sensors for damage detection in advanced fibre reinforced composites. Sensors and Their Applications Vii, 247-254.

BANHART. J. & BAUMEISTER. J., Deformation characteristics of metal foams. JOURNAL OF MATERIALS SCIENCE 33 (1998) 1431-1440

BLAZY, J. S., MARIE-LOUISE, A., FOREST, S., CHASTEL, Y., PINEAU, A., AWADE, A., GROLLERON, C. & MOUSSY, F. 2004. Deformation and fracture of aluminium foams under proportional and non-proportional multi-axial loading: statistical analysis and size effect. International Journal of Mechanical Sciences, 46, 217-244.

BOISSE. P, HAMILA. N, VIDAL-SALLÉ. E, DUMONT. F. 2011. Simulation of wrinkling during textile composite reinforcement forming. Influence of tensile, in-plane shear and bending stiffnesses. Composites Science and Technology, 71, 683-692

BOROVINSEK, M. & REN, Z. 2008. Computational modelling of irregular open-cell foam behaviour under impact loading. Materialwissenschaft Und Werkstofftechnik, 39, 114-120.

BOUBAKAR, M. L., TRIVAUDEY, F., PERREUX, D. & VANG, L. 2002. A meso-macro finite element modelling of laminate structures Part I: time-independent behaviour. Composite Structures, 58, 271-286.

CHEN, C., LU, T. J. & FLECK, N. A. 1999. Effect of imperfections on the yielding of two-dimensional foams. Journal of the Mechanics and Physics of Solids, 47, 2235-2272.

DILLARD, T., FOREST, S. & IENNY, P. 2006. Micromorphic continuum modelling of the deformation and fracture behaviour of nickel foams. European Journal of Mechanics a-Solids, 25, 526-549.

DRUGAN, W. J. & WILLIS, J. R. 1996. A micromechanics-based nonlocal constitutive equation and estimates of representative volume element size for elastic composites. Journal of the Mechanics and Physics of Solids, 44, 497-524.

DUARTE, I. & BANHART, J. 2000. A study of aluminium foam formation - Kinetics and microstructure. Acta Materialia, 48, 2349-2362.

ELLIOTT. J. A., WINDLE. A. H., HOBDELL. J. R., EECKHAUT. G., OLDMAN. R. J., LUDWIG. W., BOLLER. E., CLOETENS. P., BARUCHEL. J., In-situ deformation of an open-cell flexible polyurethane foam characterized by 3D computed micro-tomography. JOURNAL OF MATERIALS SCIENCE **37** (2002) 1547–1555

FAZEKAS, A., DENDIEVEL, R., SALVO, L. & BRECHET, Y. 2002. Effect of microstructural topology upon the stiffness and strength of 2D cellular structures. International Journal of Mechanical Sciences, 44, 2047-2066.

GIBSON, L.J., ASHBY, M.F., 1997. Cellular Solids – Structure and Properties. Cambridge University Press, Cambridge.

GONG, L., KYRIAKIDES, S. & JANG, W. Y. 2005. Compressive response of open-cell foams. Part I: Morphology and elastic properties. International Journal of Solids and Structures, 42, 1355-1379.

GRENESTEDT, J. L. & TANAKA, K. 1998. Influence of cell shape variations on elastic stiffness of closed cell cellular solids. Scripta Materialia, 40, 71-77.

GUEDES, J. M. & KIKUCHI, N. 1990. Preprocessing and Postprocessing for Materials Based on the Homogenization Method with Adaptive Finite-Element Methods. Computer Methods in Applied Mechanics and Engineering, 83, 143-198.

GUO, Z., SHI, X, CHEN, H., PENG, X. & HARRISON, P. 2012. Mechanical Modelling of Incompressible Particle-Reinforced neo-Hookean Composites Based on Numerical Homogenisation, Journal of the Mechanics and Physics of Solids (submission Sept 2012)

HARDENACKE, V. & HOHE, J. 2009. Local probabilistic homogenization of two-dimensional model foams accounting for micro structural disorder. International Journal of Solids and Structures, 46, 989-1006.

HILL, R. 1963. Elastic Properties of Reinforced Solids - Some Theoretical Principles. Journal of the Mechanics and Physics of Solids, 11, 357-372.

HOHE, J. & BECKER, W. 2003. Geometrically nonlinear stress-strain behavior of hyperelastic solid foams. Computational Materials Science, 28, 443-453.

HONIG, A. & STRONGE, W. J. 2002. In-plane dynamic crushing of honeycomb. Part II: application to impact. International Journal of Mechanical Sciences, 44, 1697-1714.

JANG, W. Y., KRAYNIK, A. M. & KYRIAKIDES, S. 2008. On the microstructure of open-cell foams and its effect on elastic properties. International Journal of Solids and Structures, 45, 1845-1875.

JANG, W. Y., KYRIAKIDES, S. & KRAYNIK, A. M. 2010. On the compressive strength of open-cell metal foams with Kelvin and random cell structures. International Journal of Solids and Structures, 47, 2872-2883.

KORNER, C., THIES, M. & SINGER, R. F. 2002. Modeling of metal foaming with Lattice Boltzmann automata. Advanced Engineering Materials, 4, 765-769.

KOUZNETSOVA, V., BREKELMANS, W. A. M. & BAAIJENS, F. P. T. 2001. An approach to micro-macro modeling of heterogeneous materials. Computational Mechanics, 27, 37-48.

KRAYNIK, A. M. 2006. The structure of random foam. Advanced Engineering Materials, 8, 900-906.

KRAYNIK, A. M., REINELT, D. A. & VAN SWOL, F. 2003. Structure of random monodisperse foam. Physical Review E, 67.

KRAYNIK, A. M., REINELT, D. A. & VAN SWOL, F. 2004. Structure of random foam. Physical Review Letters, 93.

KRUYT, N. P. & ROTHENBURG, L. 2004. Kinematic and static assumptions for homogenization in micromechanics of granular materials. Mechanics of Materials, 36, 1157-1173.

LAROUSSI, M., SAB, K. & ALAOUI, A. 2002. Foam mechanics: nonlinear response of an elastic 3D-periodic microstructure. International Journal of Solids and Structures, 39, 3599-3623.

LI, K., GAO, X. L. & SUBHASH, G. 2006[(a)]. Effects of cell shape and strut cross-sectional area variations on the elastic properties of three-dimensional open-cell foams. Journal of the Mechanics and Physics of Solids, 54, 783-806.

LI, K., GAO, X. L. & WANG, J. 2007. Dynamic crushing behavior of honeycomb structures with irregular cell shapes and non-uniform cell wall thickness. International Journal of Solids and Structures, 44, 5003-5026.

LI, Q. M., MAGKIRIADIS, I. & HARRIGAN, J. J. 2006[(b)]. Compressive strain at the onset of densification of cellular solids. Journal of Cellular Plastics, 42, 371-392.

LI, Q. M., MINES, R. A. W. & BIRCH, R. S. 2000. The crush behaviour of Rohacell-51WF structural foam. International Journal of Solids and Structures, 37, 6321-6341.

MAIRE, E., FAZEKAS, A., SALVO, L., DENDIEVEL, R., YOUSSEF, S., CLOETENS, P. & LETANG, J. M. 2003. X-ray tomography applied to the characterization of cellular materials. Related finite element modeling problems. Composites Science and Technology, 63, 2431-2443.

MARTIN, A. R., HAYES, S. A., FERNANDO, G. F. & HALE, K. F. 1995. Impact Damage Detection in Filament Wound Tubes Utilizing Embedded Optical Fibres. Smart Sensing, Processing, and Instrumentation - Smart Structures and Materials 1995, 2444, 490-501.

MICHAILIDIS, N., STERGIOUDI, F., OMAR, H., PAPADOPOULOS, D. & TSIPAS, D. N. 2011. Experimental and FEM analysis of the material response of porous metals imposed to mechanical loading. Colloids and Surfaces a-Physicochemical and Engineering Aspects, 382, 124-131.

MIEHE, C. & KOCH, A. 2002. Computational micro-to-macro transitions of discretized microstructures undergoing small strains. Archive of Applied Mechanics, 72, 300-317.

MILLS, N. J., FITZGERALD, C., GILCHRIST, A. & VERDEJO, R. 2003. Polymer foams for personal protection: cushions, shoes and helmets. Composites Science and Technology, 63, 2389-2400.

MILTZ, J. & RAMON, O. 1990. Energy-Absorption Characteristics of Polymeric Foams Used as Cushioning Materials. Polymer Engineering and Science, 30, 129-133.

ROBERTS, A. P. & GARBOCZI, E. J. 2002. Computation of the linear elastic properties of random porous materials with a wide variety of microstructure. Proceedings of the Royal Society of London Series a-Mathematical Physical and Engineering Sciences, 458, 1033-1054.

RUAN, D., LU, G., WANG, B. & YU, T. X. 2003. In-plane dynamic crushing of honeycombs - a finite element study. International Journal of Impact Engineering, 28, 161-182.

SAADA. A. S. 1974. Elasticity, theory and applications. Pregamon unified engineering series, 16

SCHMIDT, I. 2004. Deformation induced elasto-plastic anisotropy in metal foams - modelling and simulation. International Journal of Solids and Structures, 41, 6759-6782.

SHAN, Z. H. & GOKHALE, A. M. 2001. Micromechanics of complex three-dimensional microstructures. Acta Materialia, 49, 2001-2015.

SHULMEISTER, V., VAN DER BURG, M. W. D., VAN DER GIESSEN, E. & MARISSEN, R. 1998. A numerical study of large deformations of low-density elastomeric open-cell foams. Mechanics of Materials, 30, 125-140.

SILVA, M. J. & GIBSON, L. J. 1997. Modeling the mechanical behavior of vertebral trabecular bone: Effects of age-related changes in microstructure. Bone, 21, 191-199.

SILVA, M. J., HAYES, W. C. & GIBSON, L. J. 1995. The Effects of Nonperiodic Microstructure on the Elastic Properties of 2-Dimensional Cellular Solids. International Journal of Mechanical Sciences, 37, 1161-1177.

SMIT, R. J. M., BREKELMANS, W. A. M. & MEIJER, H. E. H. 1998. Prediction of the mechanical behavior of nonlinear heterogeneous systems by multi-level finite element modeling. Computer Methods in Applied Mechanics and Engineering, 155, 181-192.

SMIT, R. J. M., 1998, Toughness of heterogeneous polymeric systems, a modelling approach, PhD thesis, Printed by Universiteitsdrukkerij TU Eindhoven, Eindhoven, The Netherlands

SONG, Y. Z., WANG, Z. H., ZHAO, L. M. & LUO, J. A. 2010. Dynamic crushing behavior of 3D closed-cell foams based on Voronoi random model. Materials & Design, 31, 4281-4289.

SWAN, C. C. 1994. Techniques for Stress-Controlled and Strain-Controlled Homogenization of Inelastic Periodic Composites. Computer Methods in Applied Mechanics and Engineering, 117, 249-267.

VANDERBURG, M. W. D., SHULMEISTER, V., VANDERGEISSEN, E. & MARISSEN, R. 1997. On the linear elastic properties of regular and random open-cell foam models. Journal of Cellular Plastics, 33, 31-&.

VORONOÏ, G., 1908. Nouvelles applications des paramètres continus à la théorie des formes quadratiques. Journal für Reine und Angewandte Mathematik 134, 198–312.

WANG, Q. C., FAN, Z. J. & GUI, L. J. 2007. Theoretical analysis for axial crushing behaviour of aluminium foam-filled hat sections. International Journal of Mechanical Sciences, 49, 515-521.

WOUTERSON, E. M., BOEY, F. Y. C., HU, X. & WONG, S. C. 2005. Specific properties and fracture toughness of syntactic foam: Effect of foam microstructures. Composites Science and Technology, 65, 1840-1850.

YOUSSEF, S., MAIRE, E. & GAERTNER, R. 2005. Finite element modelling of the actual structure of cellular materials determined by X-ray tomography. Acta Materialia, 53, 719-730.

ZHANG, X. C., LIU, Y., WANG, B. & ZHANG, Z. M. 2010. Effects of defects on the in-plane dynamic crushing of metal honeycombs. International Journal of Mechanical Sciences, 52, 1290-1298.

ZHENG, Z. J., YU, J. L. & LI, J. R. 2005. Dynamic crushing of 2D cellular structures: A finite element study. International Journal of Impact Engineering, 32, 650-664.

ZHOU, J. & SOBOYEJO, W. O. 2004. Compression-compression fatigue of open cell aluminum foams: macro-/micro-mechanisms and the effects of heat treatment. Materials Science and Engineering a-Structural Materials Properties Microstructure and Processing, 369, 23-35.

ZHU, H. X., HOBDELL, J. R. & WINDLE, A. H. 2000. Effects of cell irregularity on the elastic properties of open-cell foams. Acta Materialia, 48, 4893-4900.

ZHU, H. X., HOBDELL, J. R. & WINDLE, A. H. 2001[(a)]. Effects of cell irregularity on the elastic properties of 2D Voronoi honeycombs. Journal of the Mechanics and Physics of Solids, 49, 857-870.

ZHU, H. X., THORPE, S. M. & WINDLE, A. H. 2001[(b)]. The geometrical properties of irregular two-dimensional Voronoi tessellations. Philosophical Magazine a-Physics of Condensed Matter Structure Defects and Mechanical Properties, 81, 2765-2783.

ZHU, H. X., THORPE, S. M. & WINDLE, A. H. 2006. The effect of cell irregularity on the high strain compression of 2D Voronoi honeycombs. International Journal of Solids and Structures, 43, 1061-1078.

ZHU, H. X. & WINDLE, A. H. 2002. Effects of cell irregularity on the high strain compression of open-cell foams. Acta Materialia, 50, 1041-1052.

FIGURE CAPTIONS

Figure 1: Generation of a random cellular structure using a Voronoi tessellation method. The broken lines indicate a honeycomb pattern generated from regularly-spaced seeds (white circles). By adding perturbations to the honeycomb seeds, an alternative seeding (black stars) is used to generate a randomised structure.

Figure 2: An example of a fully periodic Voronoi structure (the central square).

Figure 3: (a) Schematic representation of a 2-D material composed of a periodic microstructure consisting of a repeated RVE. (b) Two-dimensional RVE with applied PBC showing counterpart nodes on opposing faces.

Figure 4: Example of determination of contact strain (for an RVE with high degree of irregularity, α = 50).

Figure 5: Single size RVE (about 150 cells) with different degree of irregularities with same size and material specifications.

Figure 6: RVE 1X150, 4X150, 9X150 and 16X150 with 150, 600, 1350 and 2400 cells respectively.

Figure 7: The average simulation cost of each RVE size per 5% compression.

Figure 8: Effect of RVE size on reduced secant modulus at 1% and 5% compressive strain using α=20.

Figure 9: Effect of degree of irregularity on secant modulus of the 1x150 cell RVEs.

Figure 10: Averaged reduced stress-strain curves for RVEs of different size and α = 20. The form of the plateau stress region is sensitive to the size of RVE. Densification strain (OSD) and contact strain (CS) are indicated in the figure. Error bars indicate 1 standard deviation of 10 simulations.

Figure 11: Averaged reduced Stress-Strain curves for 1x150 RVE with increasing α.

Figure 12: Onset strain of densification and contact strains for RVEs with different size but the same degree of irregularity (α=20).

Figure 13: Onset strain of densification and contact strain for RVEs with varying α. Open points correspond to an RVE of size 1X150 cells, closed points correspond to an RVE of size 16X150 cells. (The closed points are offset slightly to α = 22 and 52 for clarity, though they still correspond to α = 20 and 50).

Figure 14: Average reduced stress – strain curve for the largest RVE when α = 50.

Figure A1: Schematic representation of four nodded 3D shell-based RVE based on 2D beam-based RVE where the shell width is 10 times than beam and shell thickness.

Figure A2: Comparison between implicit simulation using beam elements and explicit simulations using shell elements, here α = 20 and the RVE size is 1x150 cells.

Video 1: A typical simulation of the compression of a 1x150 cell RVE, here with α = 20, is shown in Video 1. The video shows the deformation of the microstructure of an identical RVE simulated both with self-contact (left) and without self-contact (right). The corresponding reduced stress verses strain curves are plotted above, the circles (o) are associated with the simulation with self-contact, the stars (*) are associated with simulations without self-contact.

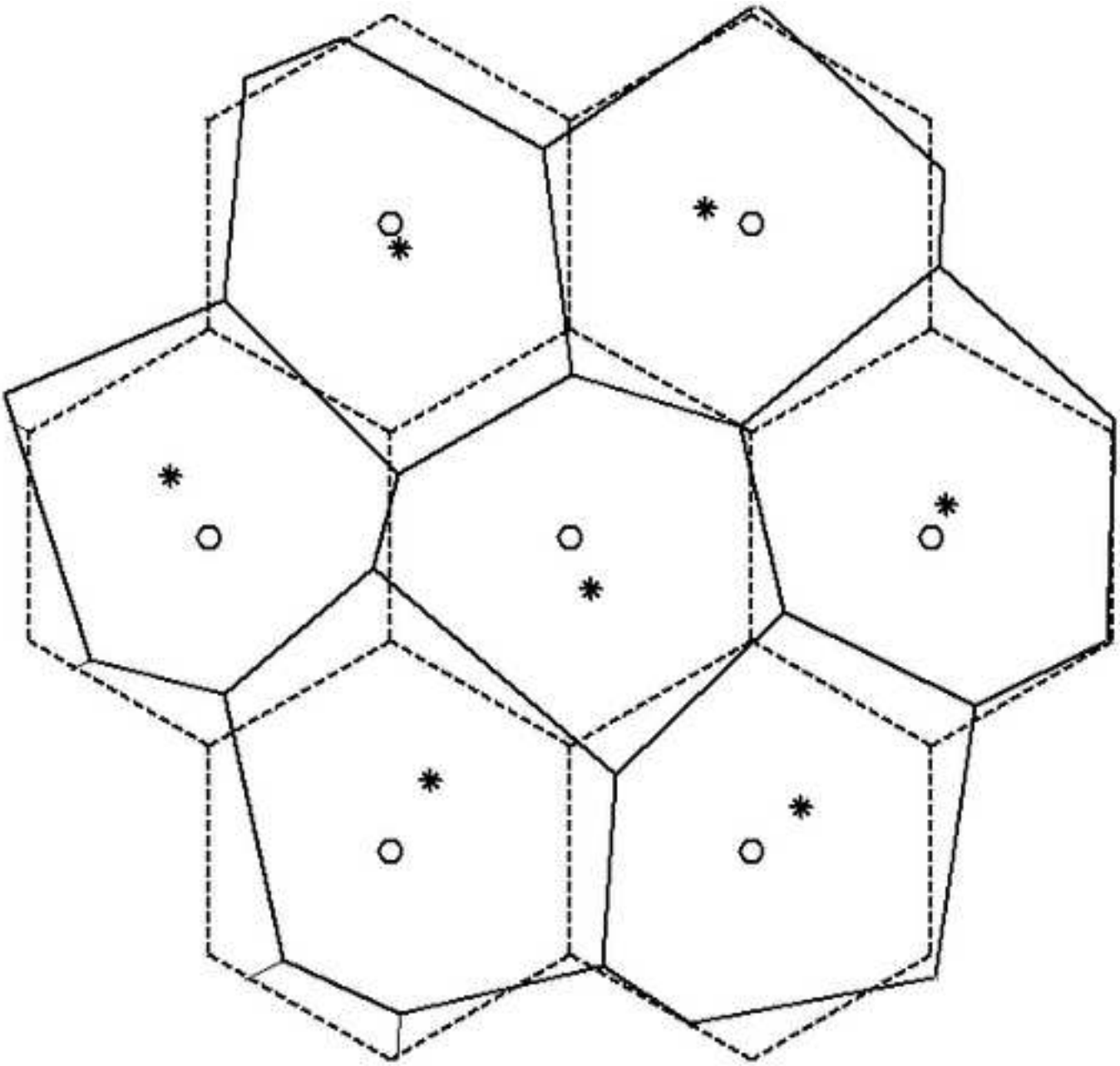

Figure 1: Generation of a random cellular structure using a Voronoi tessellation method. The broken lines indicate a honeycomb pattern generated from regularly-spaced seeds (white circles). By adding perturbations to the honeycomb seeds, an alternative seeding (black stars) is used to generate a randomised structure.

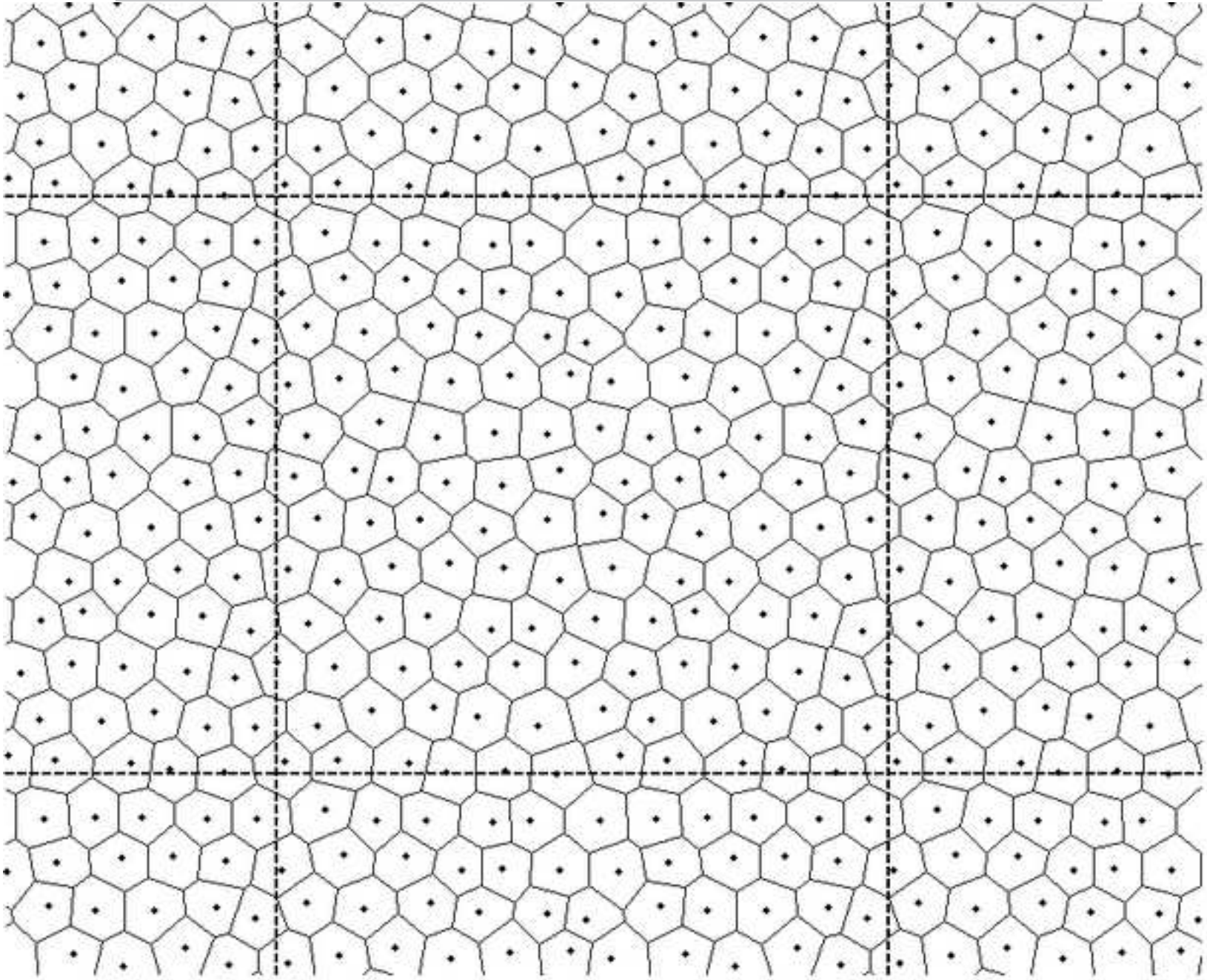

Figure 2: An example of a fully periodic Voronoi structure (the central square)

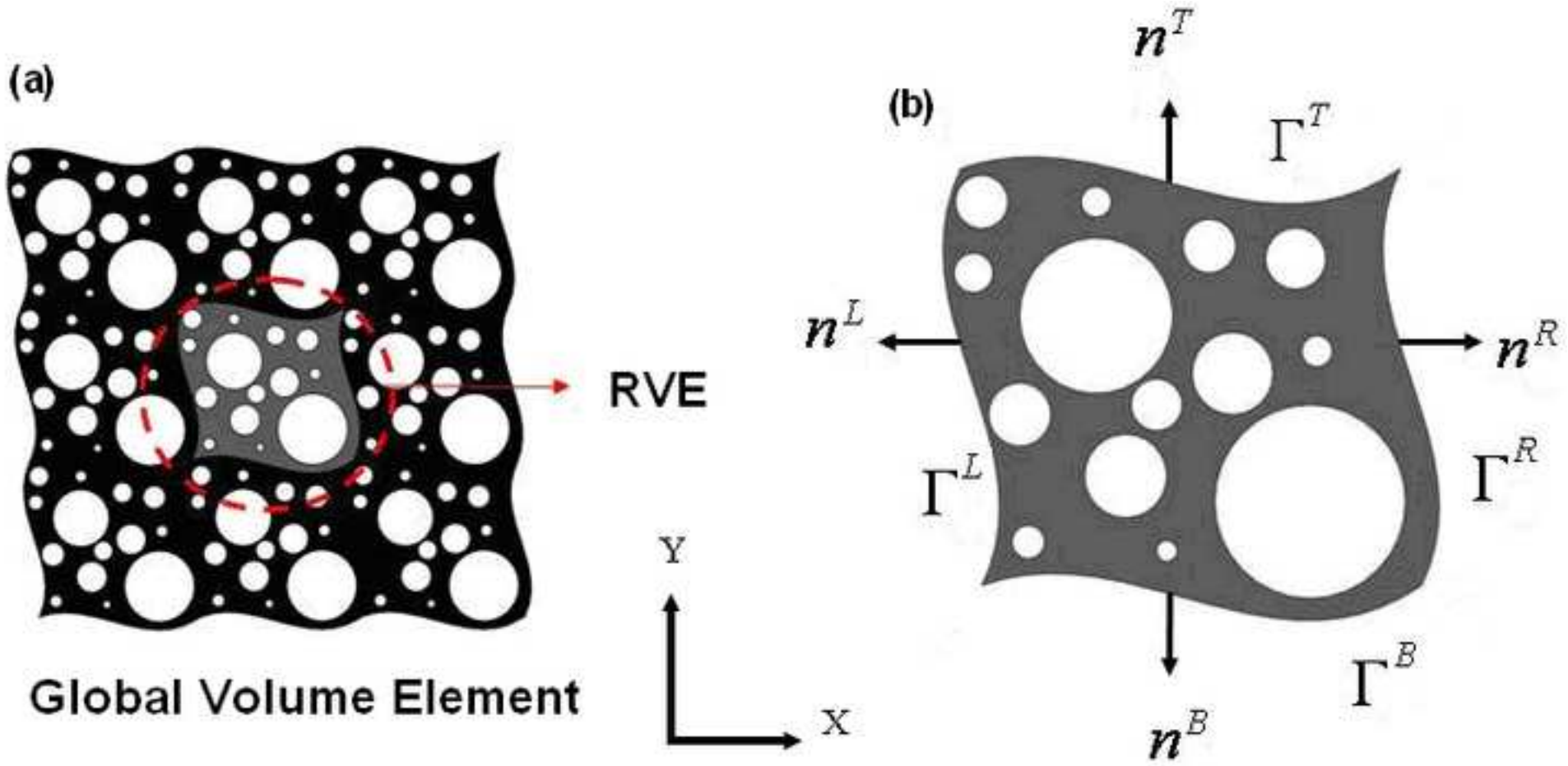

Figure 3: (a) Schematic representation of a 2-D material composed of a periodic microstructure consisting of a repeated RVE. (b) Two-dimensional RVE with applied PBC showing counterpart nodes on opposing faces.

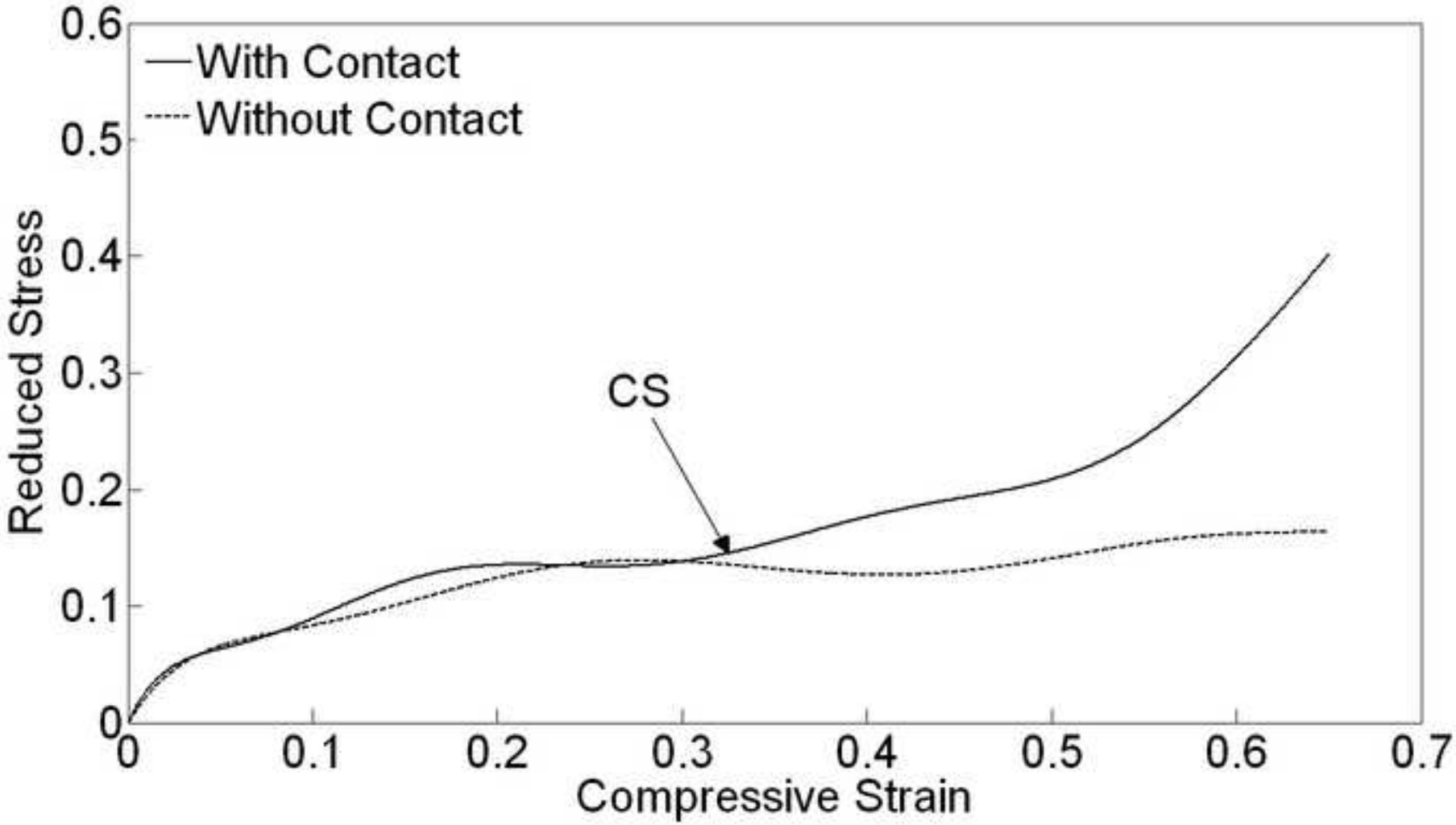

Figure 4: Example of determination of contact strain (for an RVE with high degree of irregularity, $\alpha = 50$).

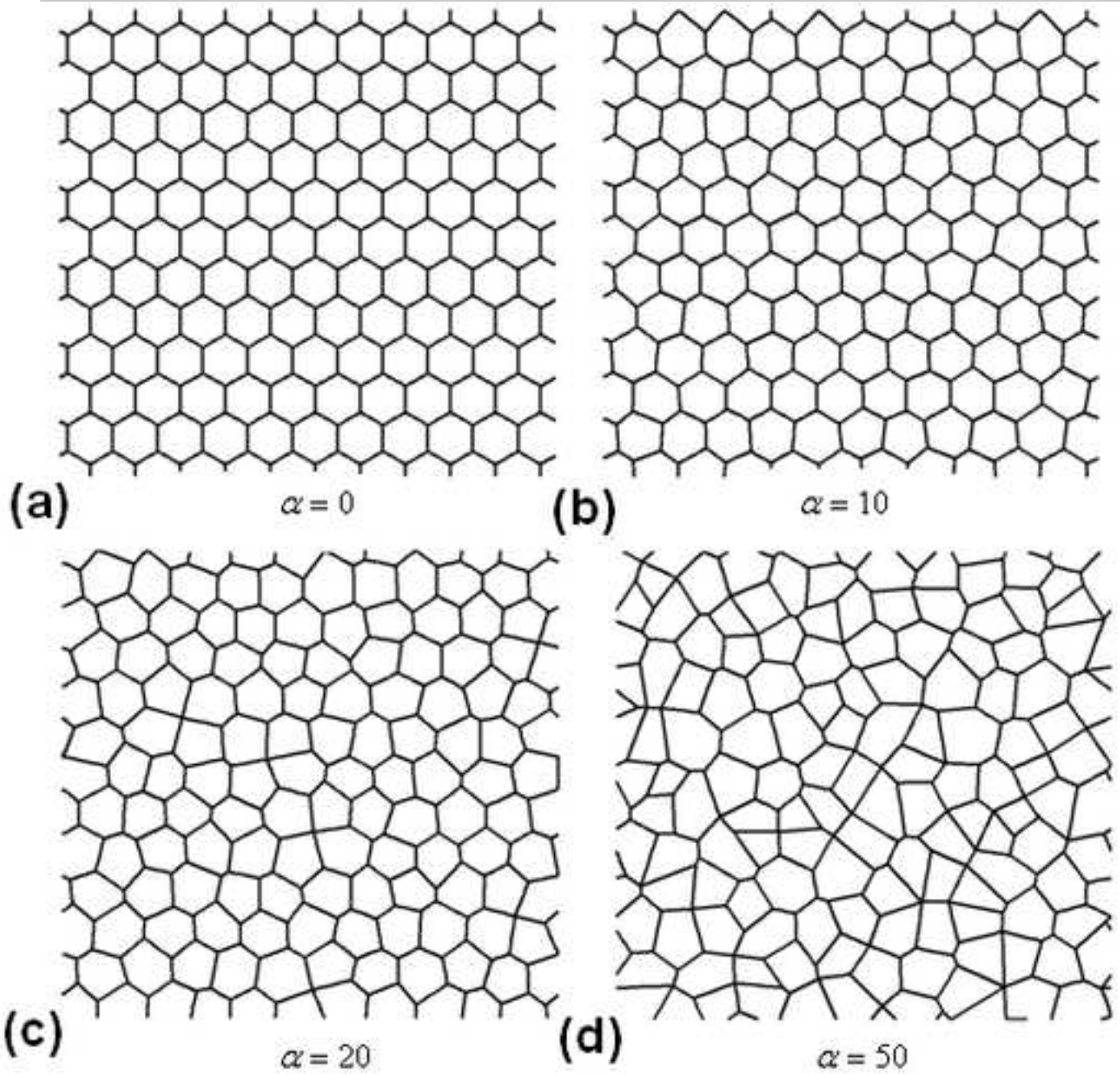

Figure 5: Single size RVE (about 150 cells) with different degree of irregularities with same size and material specifications

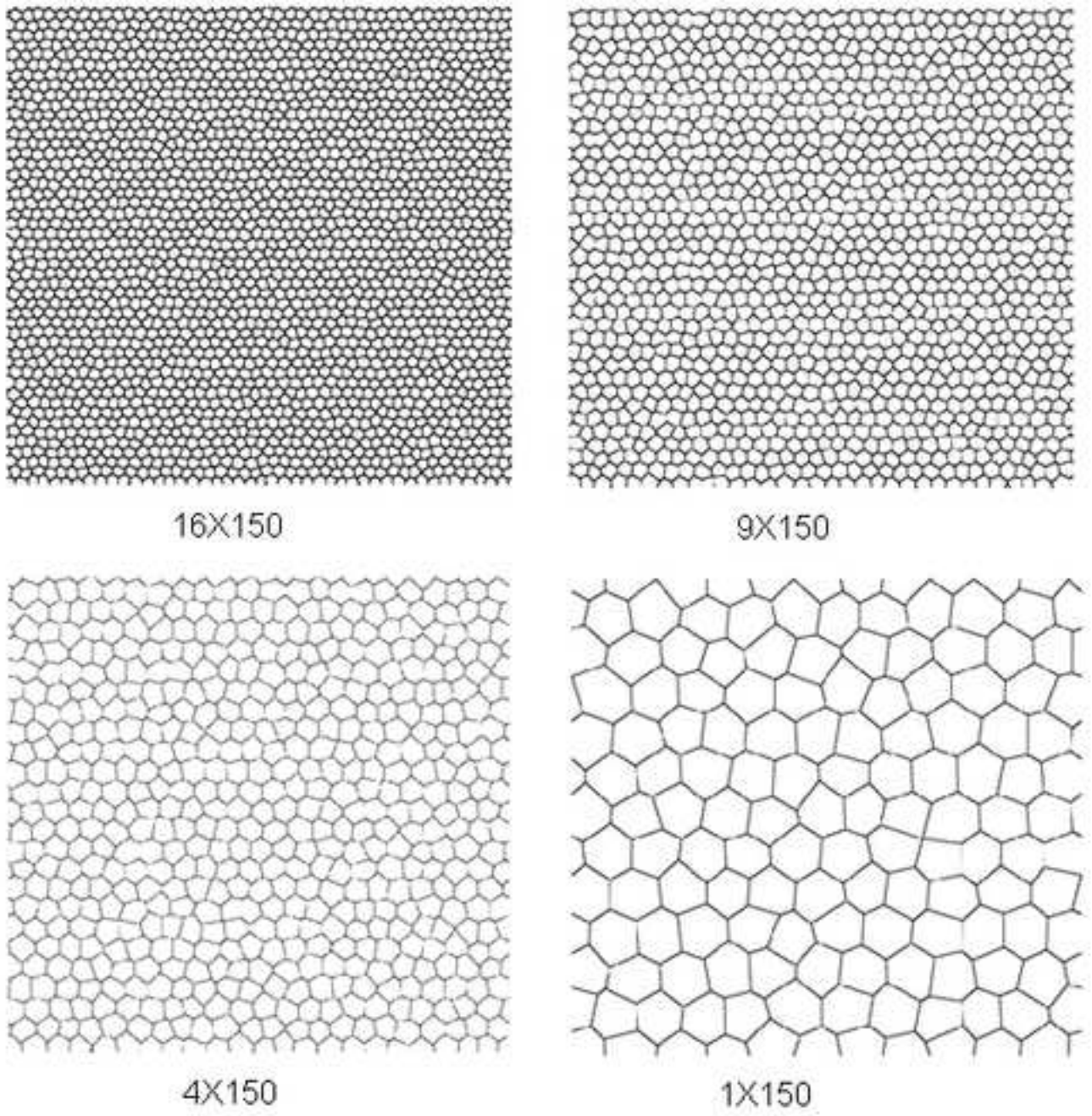

Figure 6: RVE 1X150, 4X150, 9X150 and 16X150 with 150, 600, 1350 and 2400 cells respectively.

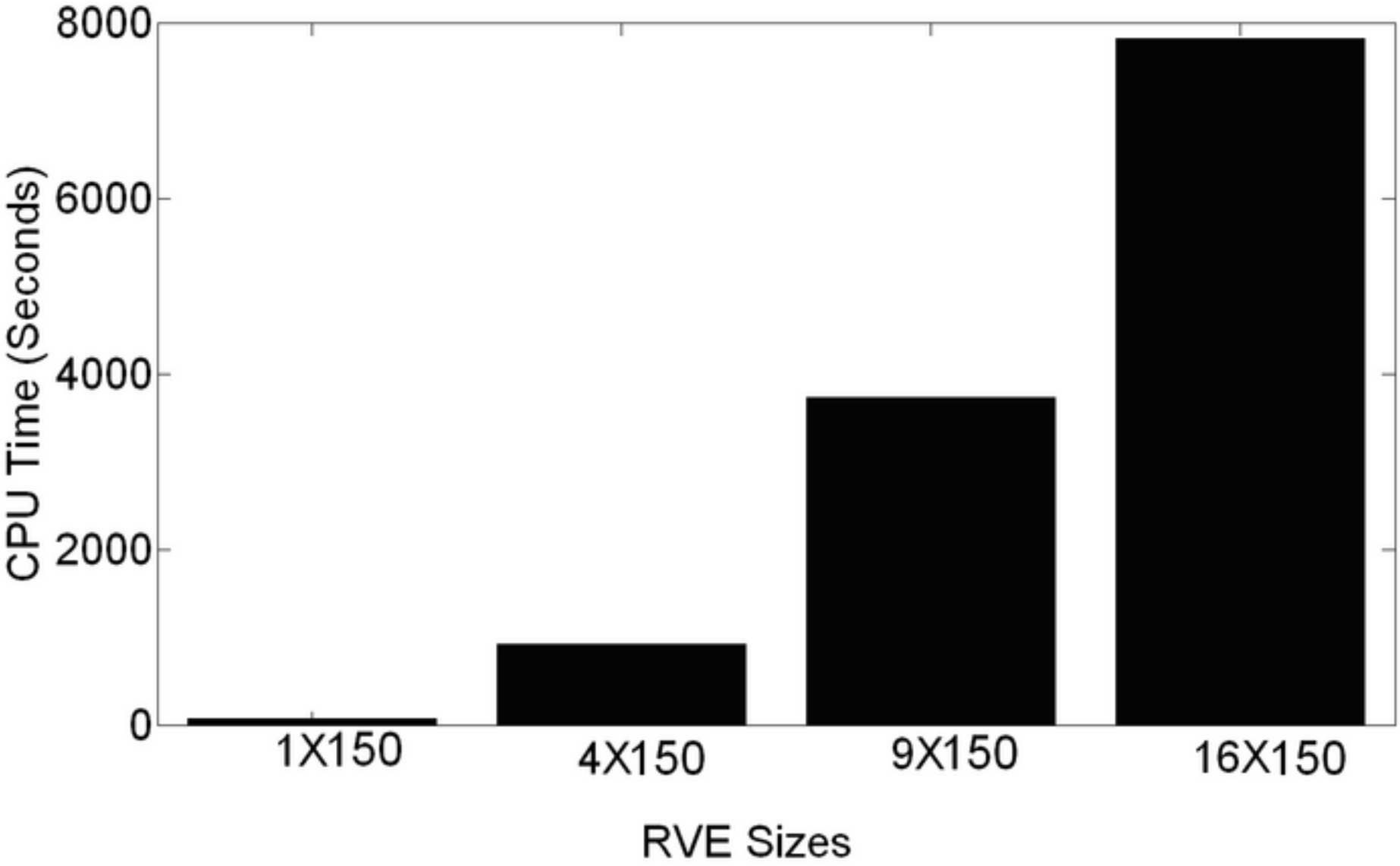

Figure 7: The average simulation cost of each RVE size per 5% compression

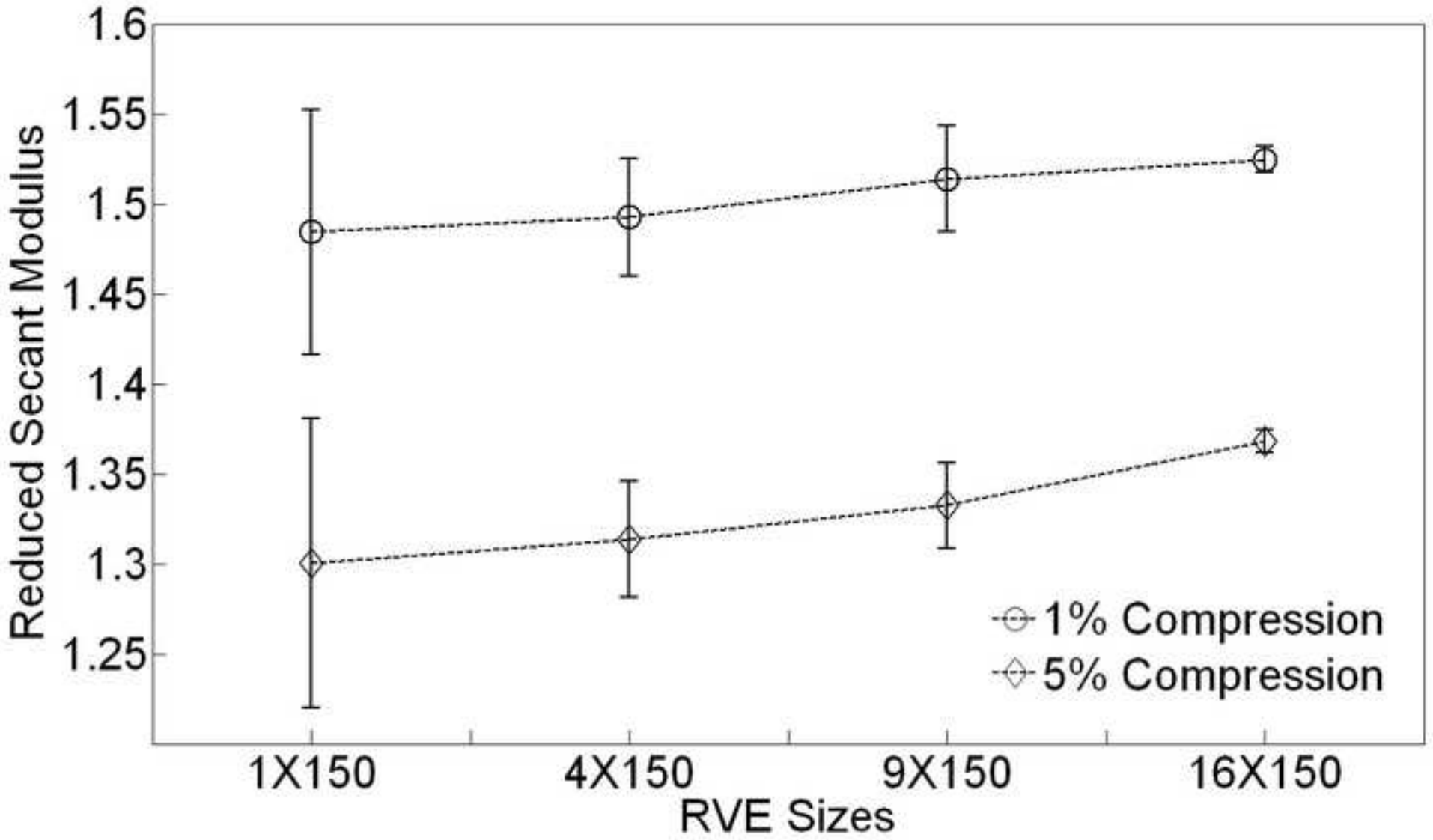

Figure 8: Effect of RVE size on reduced secant modulus at 1% and 5% compressive strain using α=20.

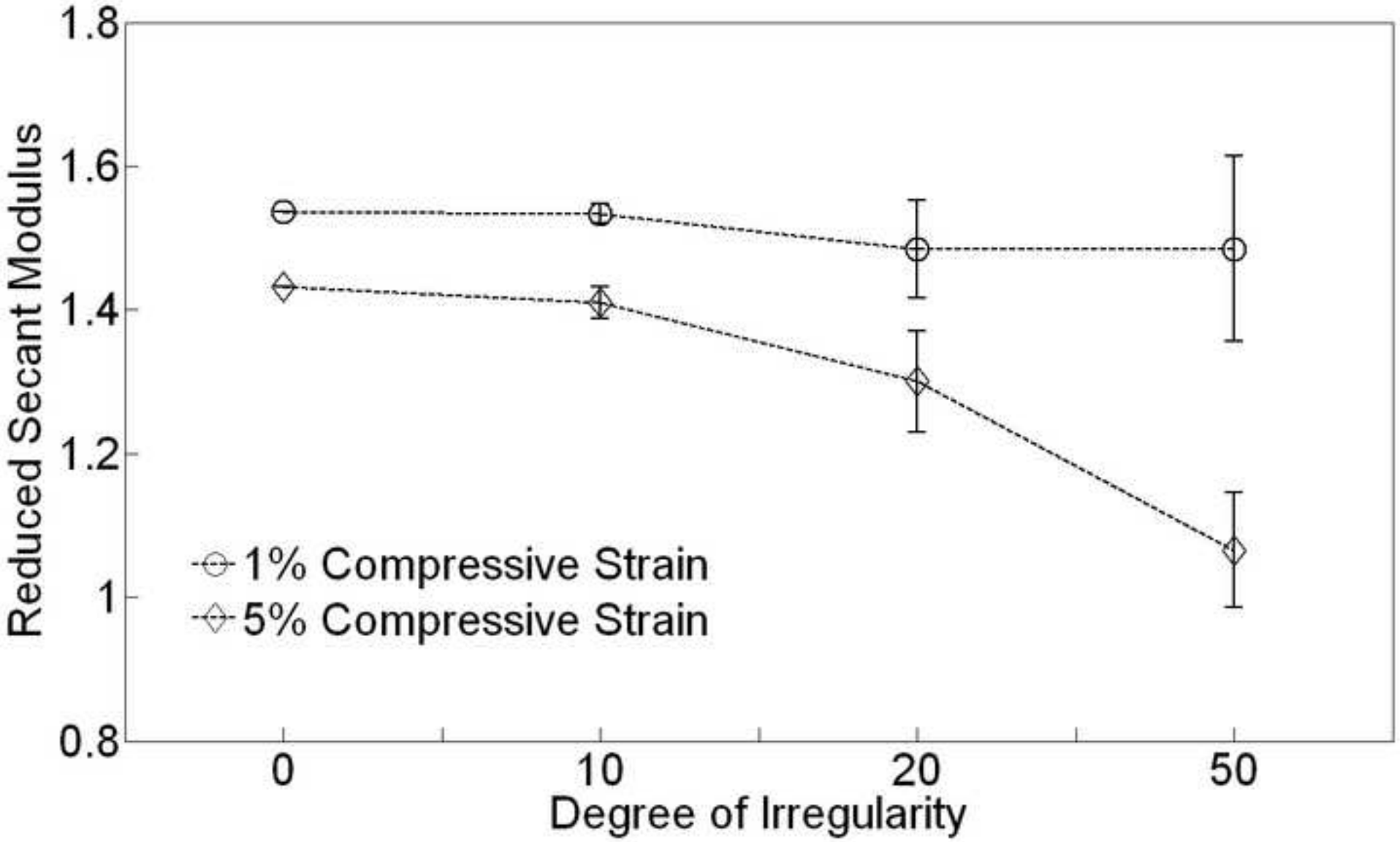

Figure 9 : Effect of degree of irregularity on secant modulus of the 1x150 cell RVEs.

Figure(s)

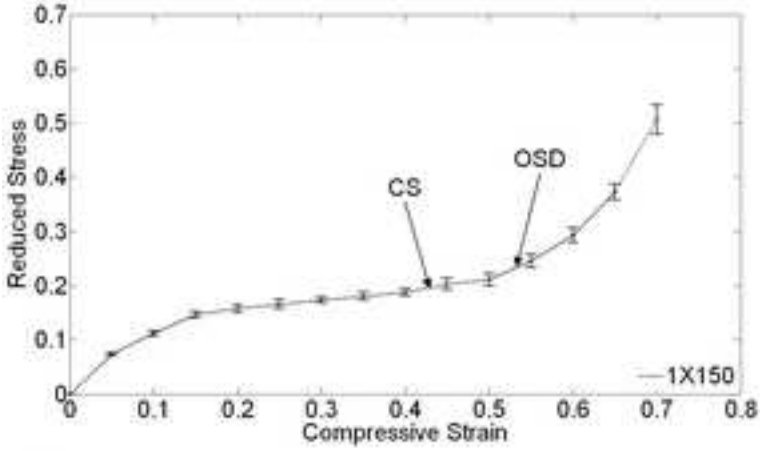

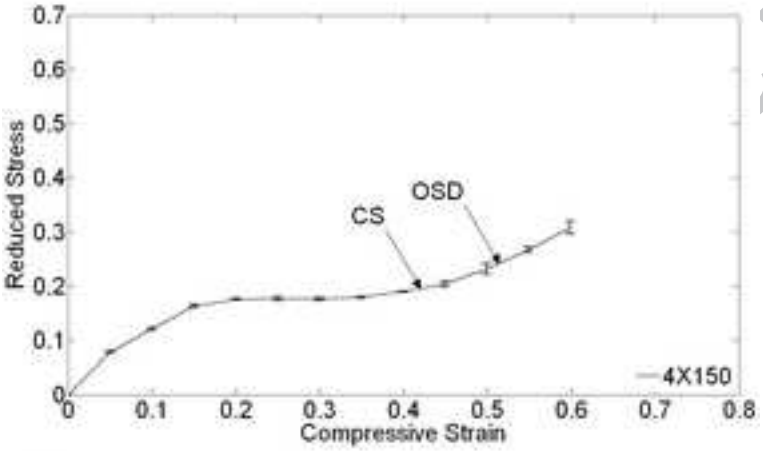

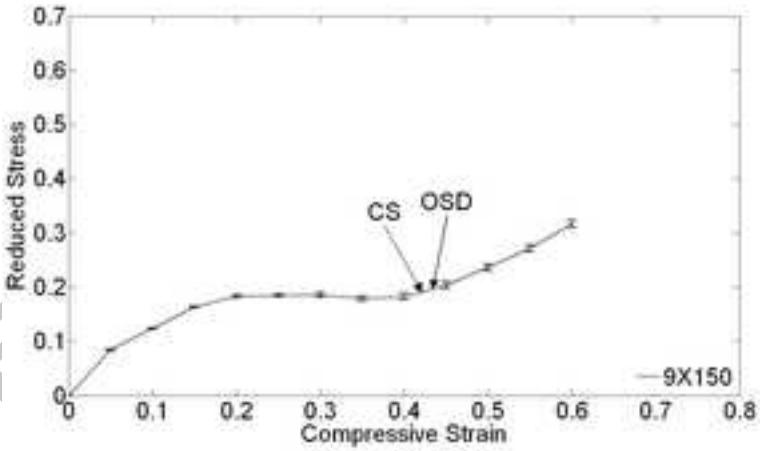

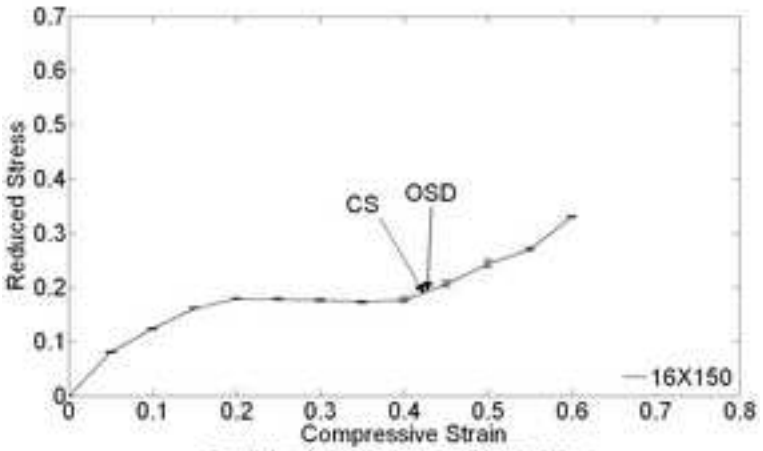

Figure 10: Averaged reduced stress-strain curves for RVEs of different size and $\alpha = 20$. The form of the plateau stress region is sensitive to the size of RVE. Densification strain (OSD) and contact strain (CS) are indicated in the figure. Error bars indicate 1 standard deviation of 10 simulations.

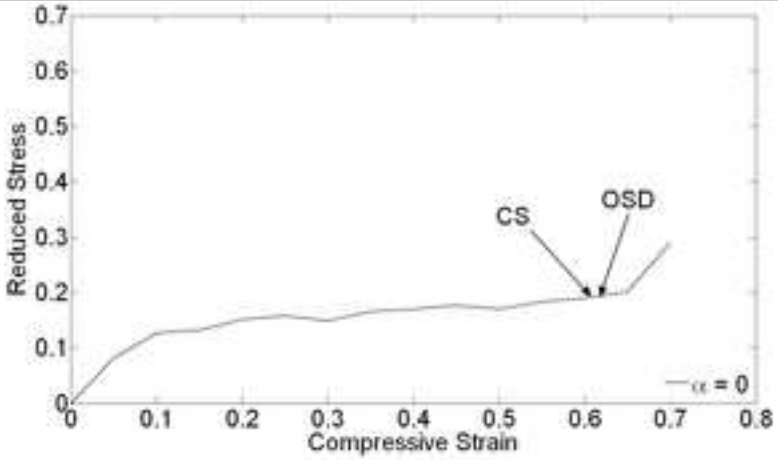

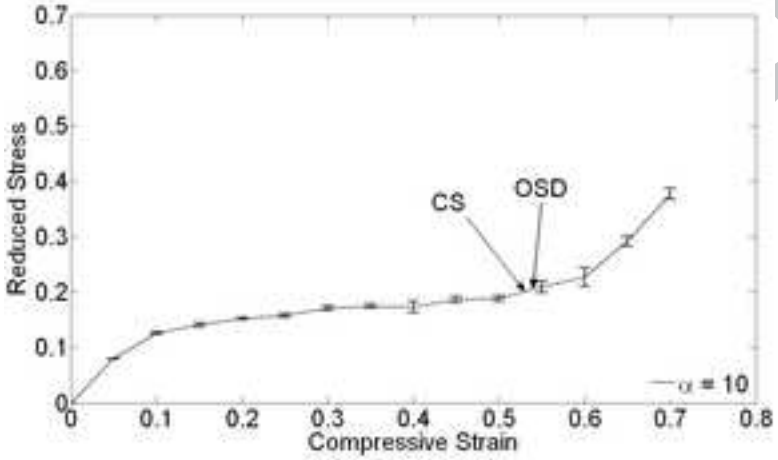

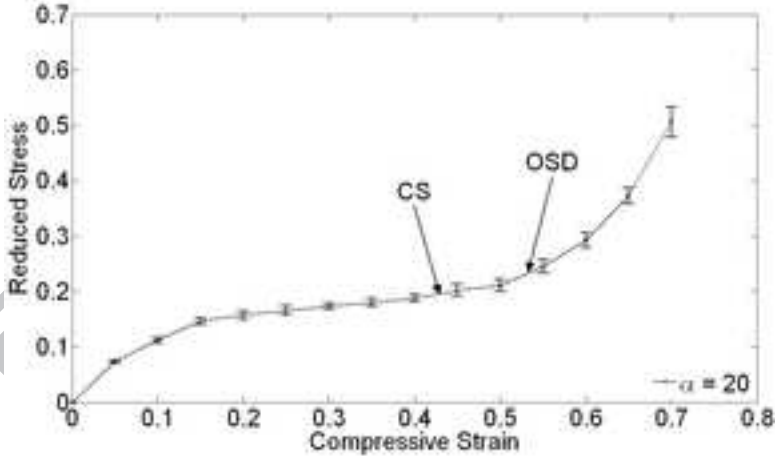

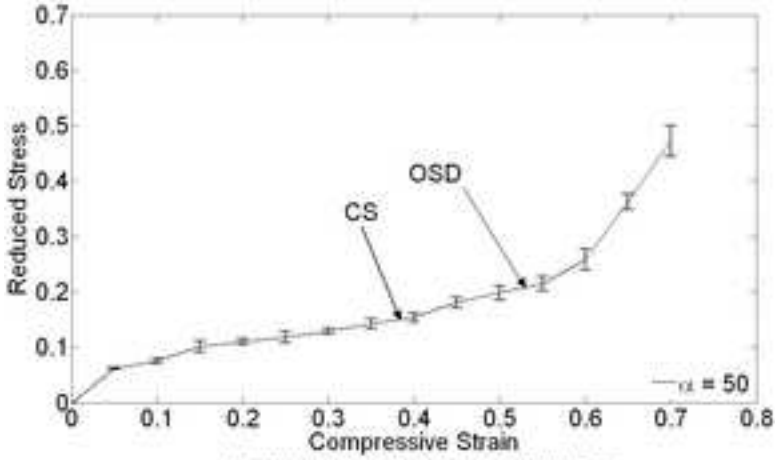

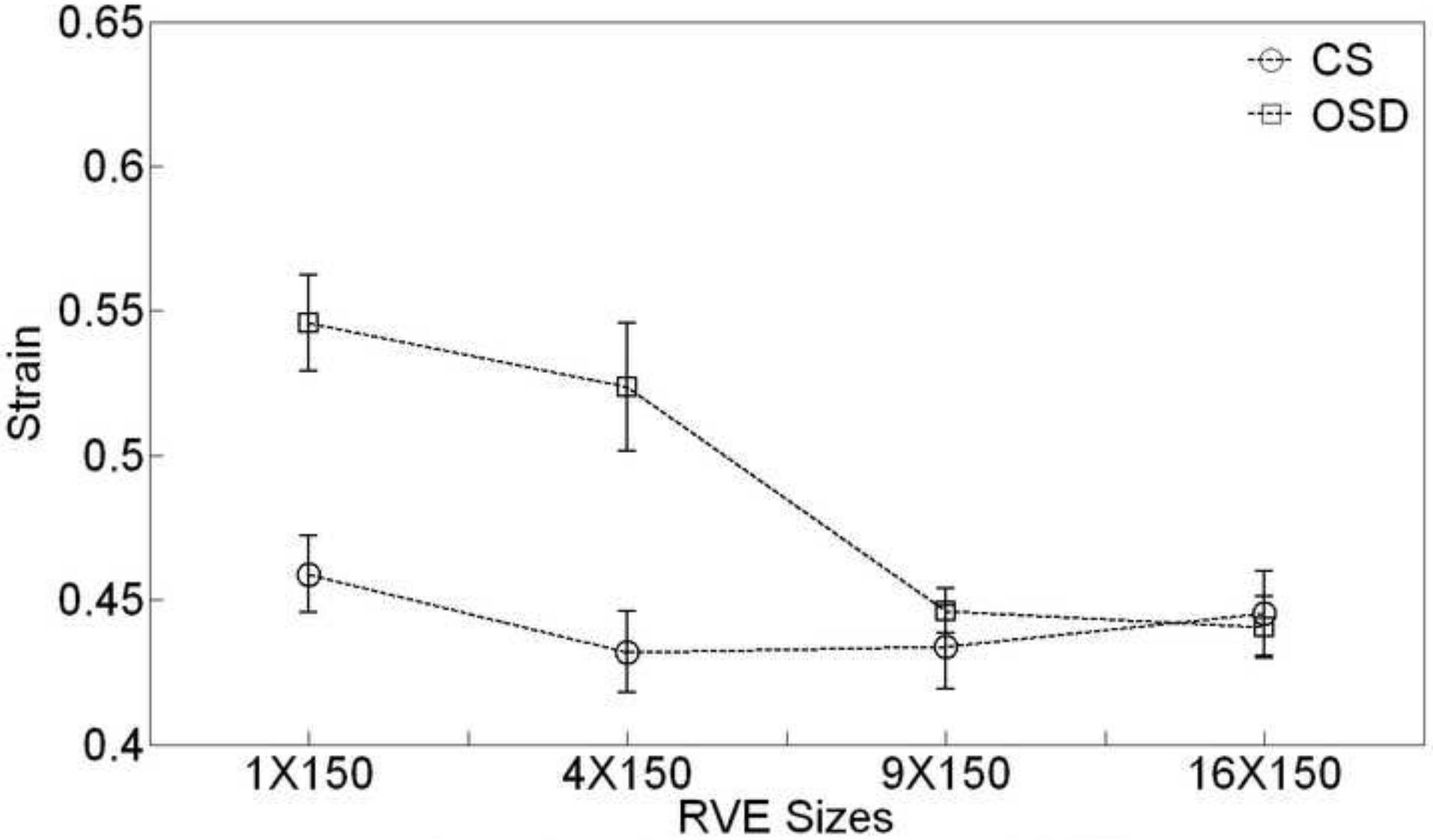

Figure 12: Onset strain of densification and contact strains for RVEs with different size but the same degree of irregularity (α=20).

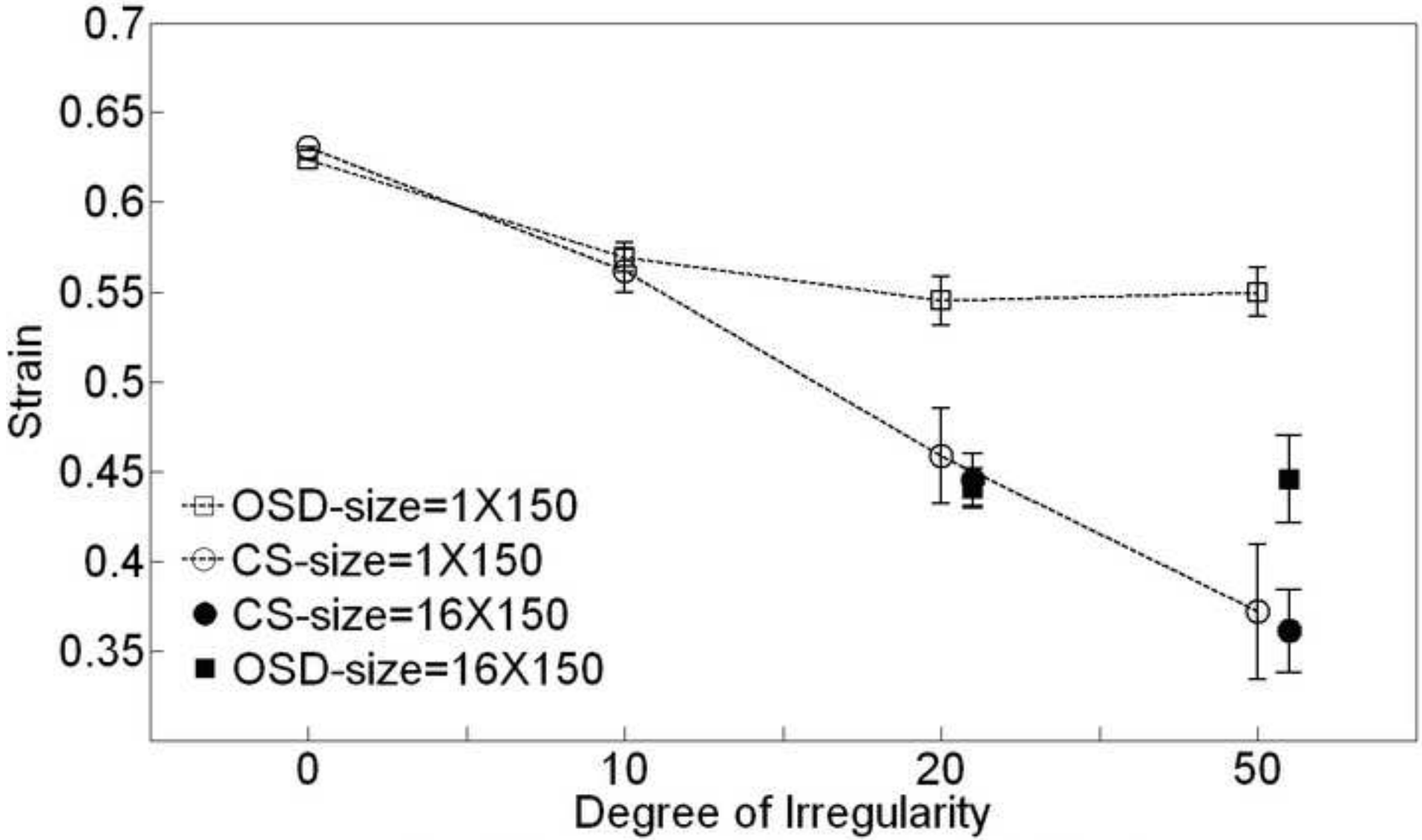

Figure 13: Onset strain of densification and contact strain for RVEs with varying α. Open points correspond to an RVE of size 1X150 cells, closed points correspond to an RVE of size 16X150 cells. (The closed points are offset slightly to α = 22 and 52 for clarity, though they still correspond to α = 20 and 50).

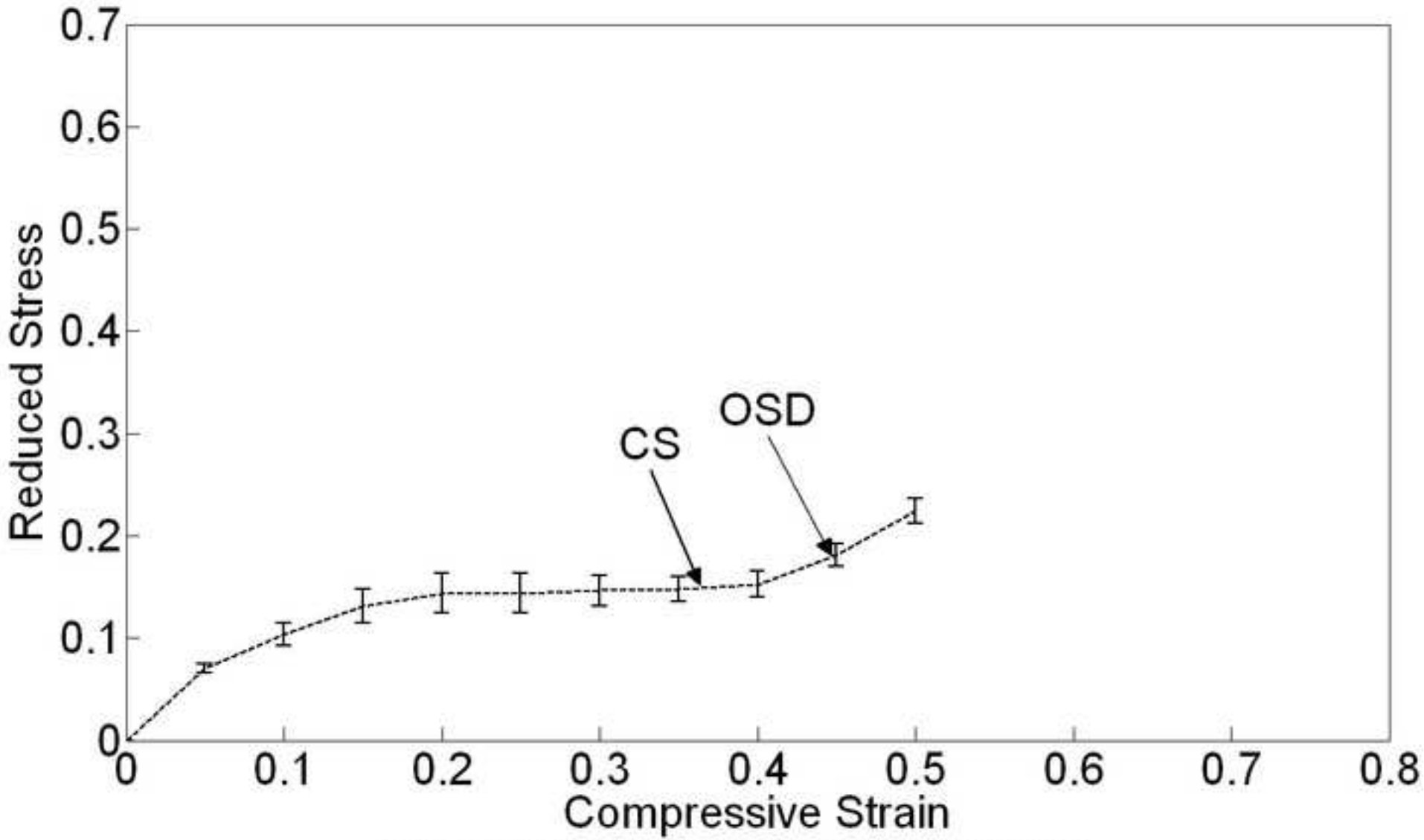

Figure 14: Average reduced stress – strain curve for the largest RVE when $\alpha = 50$.

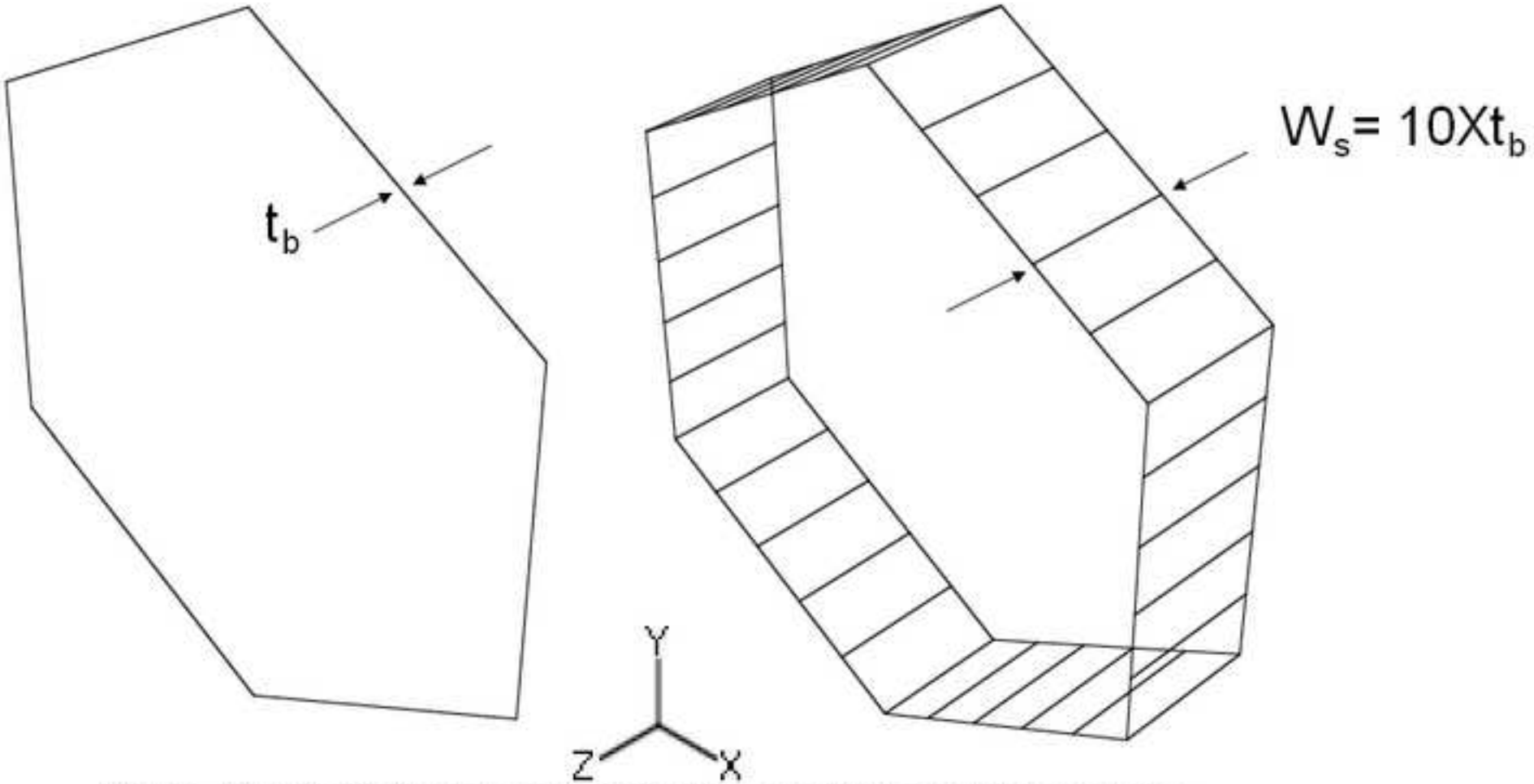

Figure A1: Schematic representation of four nodded 3D shell-based RVE based on 2D beam-based RVE where the shell width is 10 times than beam and shell thickness.

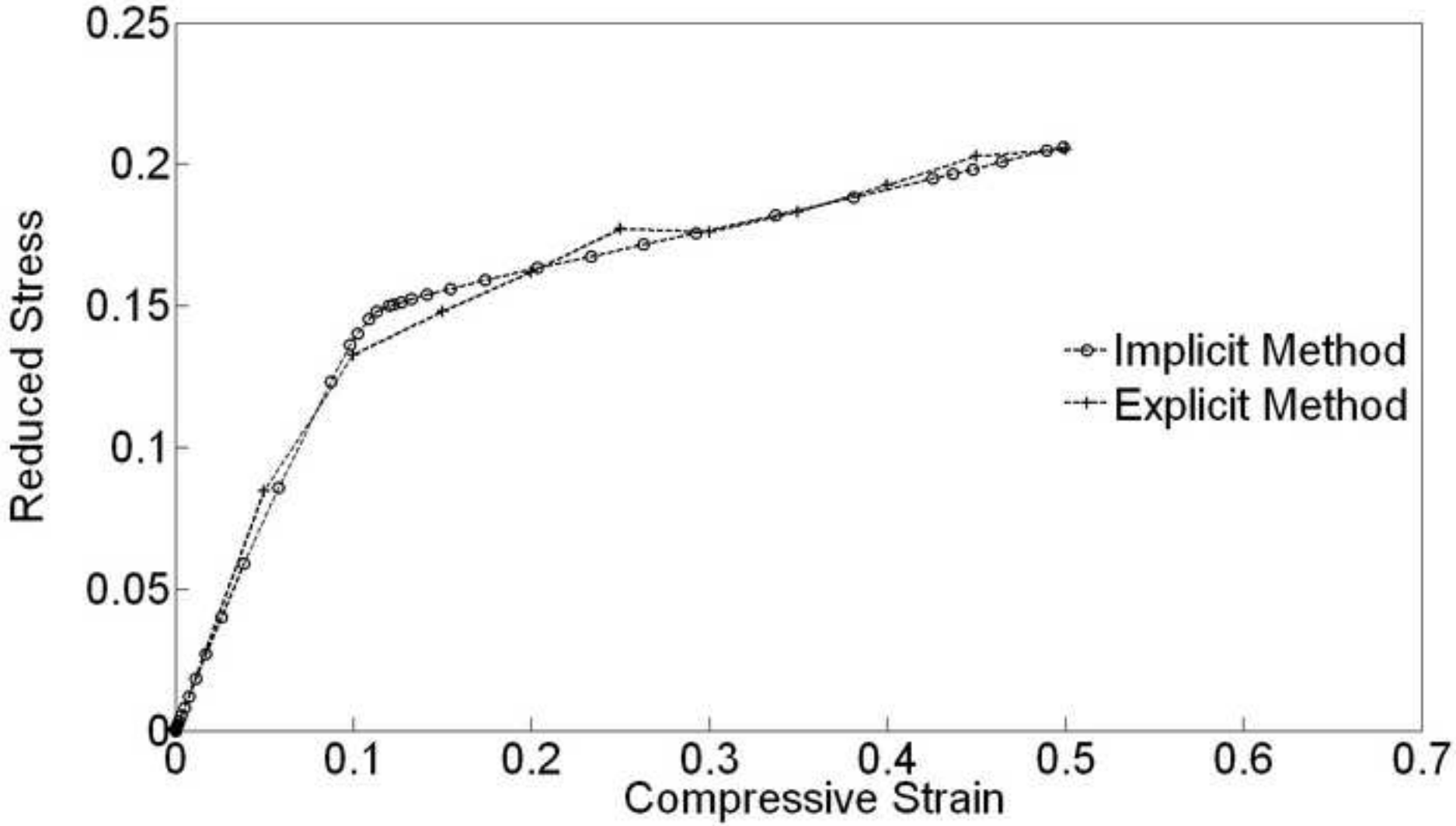

Figure A2: Comparison between implicit simulation using beam elements and explicit simulations using shell elements, here α = 20 and the RVE size is 1x150 cells.

Highlights of the paper

- The main aim of this investigation is to study the effect of combining both a periodic boundary condition and self-contact within the foam microstructure in modelling 2-D cellular structures
- The microstructure has been modelled using structural finite elements (beam and shell), use of beam-equivalent shell elements has enabled more accurate modelling of the self-contact within the microstructure
- By including self-contact within the material's microstructure the response of the foam beyond the onset strain of densification has been predicted
- We introduced a new characteristic strain, referred to here as the 'contact strain' and find that the onset strain of densification in larger RVEs can be predicted by the contact strain in small RVEs; an observation that can lead to a drastic improvement in computational efficiency when aiming to predict the onset strain of densification, by more than 100 times